AN ABSTRACT OF THE THESIS OF

Andrew G. Bryenton for the degree of Master of Science in Chemical Engineering presented on November 20, 2007.
Title: Heat Balance of Alcoves on the Willamette River, Oregon.

Abstract Approved:

Roy Haggerty

Alcoves in some river systems are cooler than the mainstem of the river and provide thermal refugia for aquatic species. An energy balance and sensitivity analysis on 3 alcoves in the Willamette River, Oregon indicate that alcove size and alcove flux determine the degree to which meteorological conditions affect the alcove water temperature. Large alcoves with a low alcove flux and large surface area are more sensitive to meteorological conditions (i.e., shade and wind). Small alcoves with a high alcove flux and small surface area are more sensitive to the temperature of emerging subsurface water than to meteorological conditions. The temperature of hyporheic water relative to the mainstem is determined by its residence time; longer flow paths disperse the diurnal signal and move hyporheic water into equilibrium with mean seasonal or annual subsurface temperatures. Floodplain restoration may increase alcove population in a river system thereby making it a potential credit trading tool for mitigating excess thermal loading in a heat stressed river.

Heat Balance of Alcoves on the Willamette River, Oregon

by
Andrew G. Bryenton

A THESIS

submitted to

Oregon State University

in partial fulfillment of
the requirements for the
degree of

Master of Science

Presented November 20, 2007
Commencement June 2008

Master of Science thesis of Andrew G. Bryenton presented on November 20, 2007.

APPROVED:

_____

Major Professor, representing Chemical Engineering

_____

Head of the School of Chemical, Biological, and Environmental Engineering

_____

Dean of the Graduate School

I understand that my thesis will become part of the permanent collection of Oregon State University libraries. My signature below authorizes release of my thesis to any reader upon request.

_____

Andrew G. Bryenton, Author

ACKNOWLEDGEMENTS

"One final paragraph of advice: Do not burn yourself out. Be as I am-a reluctant enthusiast... a part time crusader, a half-hearted fanatic. Save the other half of yourselves and your lives for pleasure and adventure. It is not enough to fight for the land; it is even more important to enjoy it. While you can. While it is still there. So get out there and mess around with your friends, ramble out yonder and explore the forests, encounter the grizz, climb the mountains. Run the rivers, breathe deep of that yet sweet and lucid air, sit quietly for a while and contemplate the precious stillness, that lovely, mysterious and awesome space. Enjoy yourselves, keep your brain in your head and your head firmly attached to your body, the body active and alive, and I promise you this much: I promise you this one sweet victory over our enemies, over those deskbound people with their hearts in a safe deposit box and their eyes hypnotized by desk calculators. I promise you this: you will outlive the bastards."

-Edward Abbey

This work was supported by funding from EPA Science to Achieve Results (STAR) Program for research grant X3832205.

TABLE OF CONTENTS

Page

LIST OF FIGURES

Figure Page

LIST OF TABLES

LIST OF APPENDICIES

Appendix Page

LIST OF APPENDIX FIGURES

LIST OF APPENDIX FIGURES (Continued)

Figure Page

LIST OF APPENDIX FIGURES (Continued)

Figure Page

LIST OF APPENDIX TABLES

Heat Balance of Alcoves on the Willamette River, Oregon

1. INTRODUCTION

Elevated summer water temperatures in the mainstem of a river cause several species of fish to seek out cooler temperatures found in some off channel habitat (OCH) (*Arscott et al.*, 2001; *Landers et al.*, 2002). OCH includes features such as alcoves where water temperature may differ significantly from that of the mainstem (*Fernald et al.*, 2006). OCH that is 2 ^{o}C cooler than the mainstem at the time of the mainstem's maximum daily temperature is classified in Oregon as Cold Water Refugia (CWR) (*ODEQ*, 2006). Aquatic wildlife, especially young and migrating fish, seek out OCH and CWR to avoid warm water, find food and shelter, and to rest (*Ebersole et al.*, 2003a; *Landers et al.*, 2002).

Due to the detrimental effects of anthropogenic heat loading in the Willamette River, the Oregon Department of Environmental Quality (ODEQ) has implemented a Total Maximum Daily Load (TMDL) for thermal pollution in the Willamette Basin (*ODEQ*, 2006). The Upper Willamette River has been assigned temperature limits, 18 ^{o}C in the summer and 13 ^{o}C in the winter, above which the water quality is considered impaired.

TMDL's are included under the National Pollution Discharge Elimination System (NPDES), which requires a permit to discharge effluent into a river. Because increased stream temperatures are partially due to point sources such as wastewater treatment plants (*Kinouchi*, 2007; *Kinouchi et al.*, 2007), Oregon point source operators permitted by the NPDES must now implement scientifically valid and effective solutions to maintain

compliance with the temperature TMDL. Solutions must account for the needs of those who live near the river, and the organisms that live in the river.

1.1 Thermal Loading Mitigation Strategies

NPDES permittees have multiple ways to reduce their thermal loading, ranging from large scale engineered projects to floodplain restoration. One engineered solution is to regulate flow of the river with a flood control dam and reservoir. For example, the Cougar Dam on the McKenzie River, a tributary of the Willamette, was retrofitted with a temperature control structure that draws water from different depths of the reservoir to take advantage of the natural thermal stratification. This makes it possible to control the temperature of reservoir outflow and aid in maintaining a natural thermal regime in the river. Other engineered solutions include piping effluent to floodplains (*Farthing*, 2006), or through large refrigerators as well as gravel augmentation in the river (*Burkholder*, 2007). Some methods have proven infeasible (*Farthing*, 2006), while others are undesirable because of associated economic, environmental, political, and social concerns.

Floodplain restoration is another method that can be used to reduce thermal loading by increasing floodplain interactions, riparian areas, hyporheic exchange, and shade. Restoring the natural functions of a river increases the complexity of the river system which leads to a higher degree of hyporheic exchange (*Fernald et al.*, 2001), more thermal heterogeneity (*Arscott et al.*, 2001), and a greater likelihood of CWR (*Fernald et al.*, 2006). Mitigating thermal loading in the Willamette River via floodplain restoration could provide other benefits such as: increased baseflow and slower release of flood waters (*Poff et al.*, 1997) and wildlife habitat.

An area of interest within floodplain restoration is hyporheic exchange. Increasing a river's hyporheic exchange is a potential way to increase the river's ability to buffer thermal loading. The hyporheic zone consists of areas where water from the main channel flows beneath the river bed, through gravel bars, and adjacent to the river bank, eventually returning to the stream (*Bencala*, 2005). Alternative definitions of the hyporheic zone have also been proposed (*Boulton et al.*, 1998; *White*, 1993). Hyporheic flow and groundwater flow make up subsurface flow. Of concern in this study is the role of subsurface flow, specifically hyporheic exchange, as a modifier of alcove temperature.

With current knowledge we cannot quantify the extent to which floodplain restoration and hyporheic exchange will maintain natural thermal regimes in a river system, especially systems with a large thermal mass (*Poole and Berman*, 2001). To effectively use floodplain restoration to achieve TMDL compliance a metric is required to translate floodplain restoration to thermal loading mitigation. The metric should include the other benefits derived from floodplain restoration that collectively are a net benefit to the river system. If the metric could translate the area of restored floodplain to a reduction in effluent temperature at a point source, then it would satisfy the requirements of the TMDL and NPDES permit. A metric that has the potential to be both scientifically effective and socially, politically, and economically acceptable is CWR. The advantage of using CWR as a metric is the ability to quantify the benefit of floodplain restoration to the river by measuring the abundance or richness of aquatic organisms (i.e., fish) using the CWR. Due to the potential for CWR to be used as a metric, this study examines alcoves and the processes contributing to CWR.

1.2 Energy Budget Research

For CWR to be used as a metric, we must achieve a sound hydrologic understanding of how alcoves classified as CWR are thermally created and thermally maintained. This understanding is gained by performing an energy balance on the alcove water to quantify all the heat sources and sinks acting on the water, and to quantify the sensitivity of CWR to each parameter. Past research used energy balances on small streams to predict their temperature (*Brown,* 1969), and quantify the effect of solar energy inputs to the stream (*Johnson,* 2004). In addition, energy balances were used to quantify the affect of water/stream-bed interactions (*Evans et al.,* 1998) and inter-annual variability of stream temperatures (*Webb and Zhang,* 2004). Recently, energy budgets have been applied to salmonid embryo development and habitat selection, with respect to water column and gravel bed temperatures across temporal and spatial scales (*Hannah et al.*, 2004; *Torgersen et al.*, 1999).

Accuracy and resolution of energy balances continue to increase as temperature instrumentation becomes more portable and affordable (*Johnson et al.*, 2005). Miniature thermistors (*Johnson et al.*, 2005) and fiber optic temperature sensing (*Selker et al.*, 2006a; *Selker et al.*, 2006b) have allowed characterization of river temperatures at high resolution (*Caissie*, 2006). In addition, incorporation of an energy balance into computer models allows for accurate stream temperature predictions at differing spatial and temporal levels.

1.3 Purpose of the investigation

There is a paucity of data quantifying the drivers of alcove temperature. While research has been conducted on the effect of shade on alcove temperature (*Ebersole et*

al., 2003b), this study seeks to elucidate and quantify the most important parameters that control the water temperature in an alcove. The importance of each parameter (e.g., shade and hyporheic flux) is quantified through hydrodynamic modeling and a sensitivity analysis using a hydrodynamic model (CE-QUAL-W2) to evaluate each parameter's importance to alcove temperature. We hypothesize that solar radiation is the main heat source, while shade, hyporheic flow, and cold water upwelling are the main temperature modifiers.

2. METHODS

2.1 Site Description

To investigate the processes controlling alcove temperatures, we performed a field and modeling study to characterize the hydrologic makeup of 3 alcoves on the Upper Willamette River in Oregon (Figure 1). The Willamette River is an 8th order stream that flows north through the Willamette Valley to the Columbia River. The Willamette Valley is bordered to the west by the Coast Range and to the east by the Cascade Range.

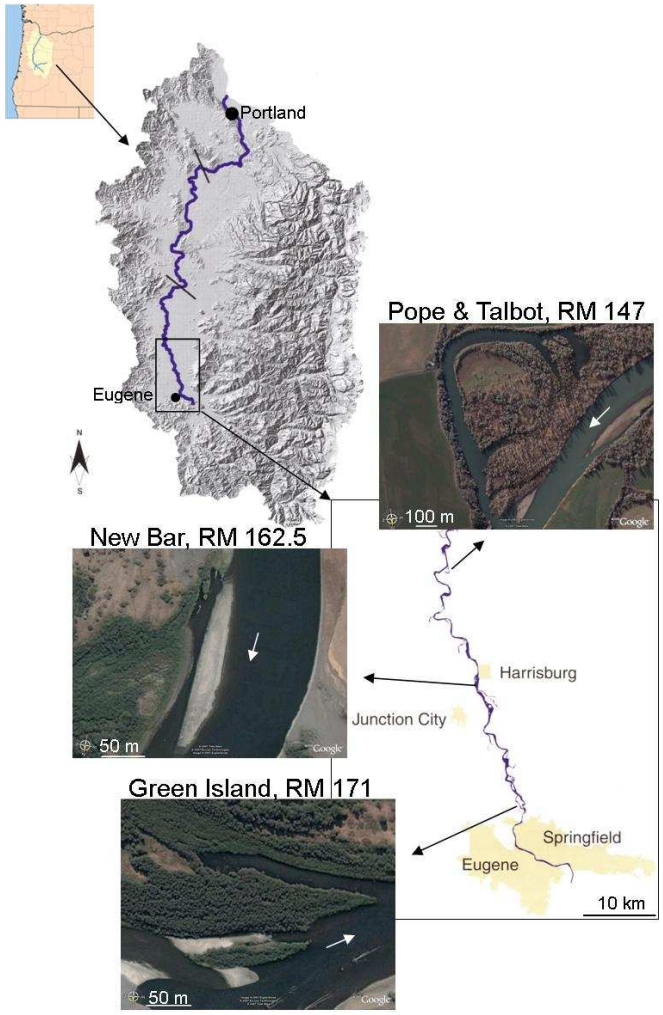

Figure 1. Study reach of the Upper Willamette River, Oregon, USA. Modified from (*Hulse et al.*, 2002).

The valley is an agriculturally intensive area due to a Mediterranean climate and to thick soils originating in the fluvial deposits of the Missoula floods and modern Willamette River (*O'Connor et al.*, 2001). Bed material of the Willamette River is predominately gravel, bounded by Holocene and Pleistocene sediments that are generally more consolidated with depth and age. The river was historically braided with a high degree of lateral movement during flashy winter flows (*Fernald et al.*, 2006; *Hulse et al.*, 2002). This created multiple side channels that were continuously abandoned and reclaimed by the river. Presently, the river has less complexity due to anthropogenic constraints such as bank hardening, revetments, channelization, and upstream flood control reservoirs that regulate discharge.

Harrisburg Bar [formerly New Bar] (Figure 2), at RM 162.5, is a young point bar alcove, approximately 200 m long, which formed during the winter flows from December, 2005 to January, 2006. Vegetation on the gravel bar consists of sparse forbes, while the bank contains young black cottonwood, *Populus trichocarpa*, (~5 m tall) that are located 20 m from the bank and provide little shade to the alcove. The elevation of the gravel bar is maximally 0.5 m above the mainstem's water surface which means the gravel bar is only exposed during summertime low flows. In addition, once releases from upstream flood control reservoirs begin in late July, the mainstem rises enough to spill over the head of the point bar and into the head of the alcove, greatly influencing the water temperature and flow rate in the alcove (Figure 2). A large log deposited longitudinally near the head of the alcove prevents incoming mainstem flow from mixing with a portion of the water at the head of the alcove. This creates a pool and allows hyporheic conditions to dominate the thermal regime at the head of the alcove. Hyporheic

flow emerges from the gravel at the head of the alcove into this pool. This is the same location where thermistor A23 was located which was used to calibrate the model and run the sensitivity analysis.

Figure 2. Harrisburg Bar site on the Willamette River, RM 162.5.

Green Island (Figure 3), the southern-most alcove in the study, is located at RM 171. Green Island is approximately 200 m long, and is located 2 km downstream of the confluence of the Willamette and McKenzie Rivers. This mature point bar alcove has extensive black cottonwood, *Populus trichocarpa*, around the perimeter. From the water surface at the head of the alcove there is a 1 m rise to the land surface. Along this rise there is a gravel seam where emerging hyporheic water flows into the alcove. Unlike Harrisburg Bar, the mainstem does not connect to the head of the alcove, indicating that

hyporheic flow comprises the majority of the water in the alcove. Model calibration and sensitivity analysis were concentrated at the same location as thermistor RW030.

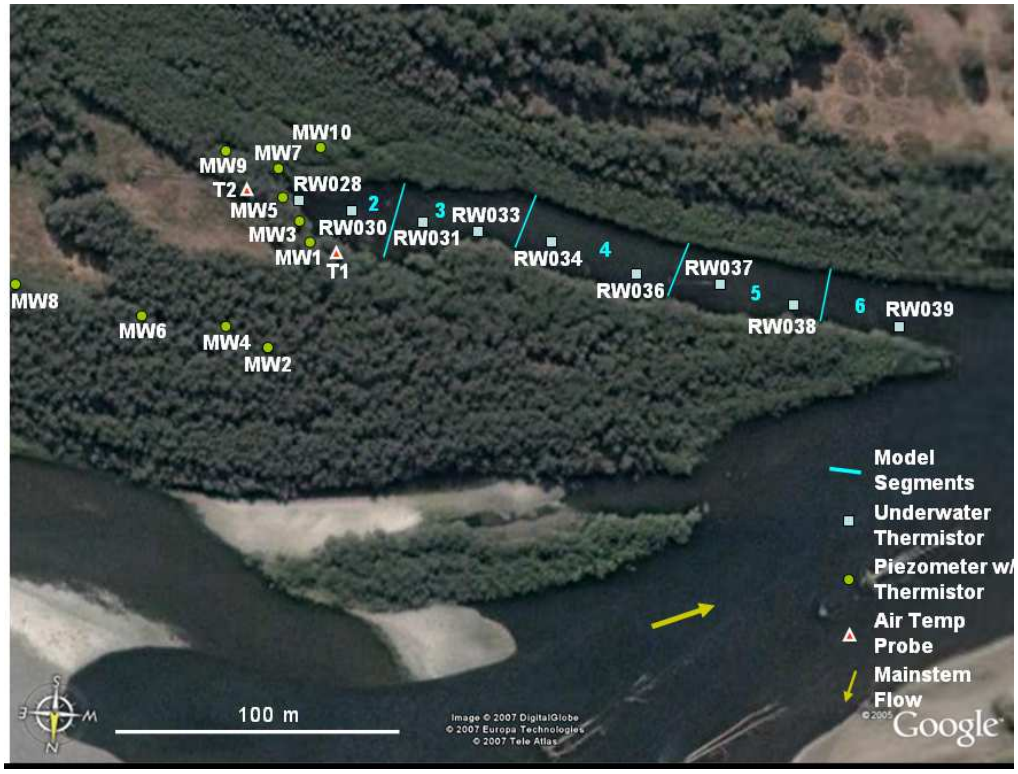

Figure 3. Green Island site on the Willamette River, RM 171.

Norwood Slough (formerly Pope and Talbot) (Figure 4), the northern-most site, at RM 145, is a disconnected, remnant side channel. This site has several features that are not present in the other alcoves. It is longer, 1537 m, and the bank is taller (3-6 m) than the banks at Harrisburg Bar and Green Island (~1 m). There is no visible movement of water in the alcove and ~50% of the alcove contains a high density of macrophytes. In addition, there is a beaver dam and pond at the head of the alcove with multiple cold water upwellings 50 m downstream of the beaver dam. The hydraulic head at the upwelling sites ranges from 5-10 cm, and water discharges at a constant temperature of ~11 ^{o}C. The model was calibrated to thermistor RW036 and a sensitivity analysis was performed at the same location as RW034.

Figure 4. Norwood Slough site on the Willamette River, RM 147.

Table 1. Sources of data.

Data	**Source**
A, cross sectional area of alcove	Measured
Q, alcove flow rate	Measured
Slope	Measured/USGS topos
D, dispersion coefficient in alcove	Calculated
H_s, solar radiation	Agriment Station
Wind speed and direction	Agriment Station
T_d, dew point temperature	Agriment Station
T_a, air temperature	Measured
T_w, alcove water temperature	Measured
T_s, sediment temperature	Estimated (*Domenico and Schwartz*, 1990)
Incoming temperature of hyporheic water	Measured
Seepage into alcove	Calculated
Hyporheic flux into alcove	Estimated through calibration
Cold water upwelling flux	Estimated through calibration
Vegetation shading	Estimated in field
Topographic shading	Estimated in field

2.2 Sampling Methods

Field data were conducted at each site from July to September, 2006 to parameterize and construct 3 models in CE-QUAL-W2. Physical properties of each site were measured, calculated, or estimated (Table 1). Measured properties included alcove bathymetry, discharge, and vegetation (Table 2). Air and water temperature were also recorded at each site for approximately 10 days.

Table 2. Site measurements.

Site Measurement	Harrisburg Bar	Green Island	Norwood Slough
Avg hydraulic conductivity of gravel bar, m/s	$7.0x10^{-4}$	$2.6x10^{-4}$	$3.9x10^{-5}$
Alcove slope, -	$7.5x10^{-4}$	$1.0x10^{-5}$	$1.0x10^{-5}$
Avg alcove width, m	19.2	23	48.7
Avg alcove depth, m	0.2	0.6	1.1
Width to depth ratio, -	87.3	41	43.6
Alcove length, m	200	205	1537
Alcove surface area, m^2	4000	5000	80000
Alcove volume, m^3	1150.7	3116.5	115148.2
Alcove flow rate, m^3/s	0.14	0.26	0.38
Alcove water velocity, m/s	0.07	0.02	0.001
Peclet # (through gravel bar), -	251	640	157
Alcove water residence time, hr	1	5.5	48-72
Vegetation surrounding alcove	small forbes on bar; sparse, ~4 m black cottonwoods on bank side	well established black cottonwoods and shrubs around alcove	well established black cottonwoods surrounding alcove
Shade density on bank	20%	50%	40%
Direct flow from mainstem	yes	no	no
Visible hyporheic flow	no	yes	no
Cold water upwelling	none	no	yes
Macrophytes	none	sparse	very thick

2.2.1 Bathymetry/Tracer Test

Cross section measurements and tracer tests were performed at each site. Five cross sections were measured in each alcove using a stadia rod and measuring tape. Initially, a doppler water velocity meter (FlowMate 2000, Marsh-McBirney, Fredrick, MA, USA) was used to measure water velocity at the surface and 1/3 depth, but the

instrument was not accurate enough to record the low velocities in the alcoves. To find each alcove's flux, tracer tests were performed by releasing rhodamine WT (Bright Dyes Liquid Concentrate Fluorescent Red) at the head of each alcove (1.742 g at Harrisburg Bar, 3.346 g at Green Island, and 12.000 g at Norwood Slough, 100% RWT). A fluorometer (Turner Designs 10-AU Sunnyvale, CA, USA) recorded the concentration of the dye as it moved out of the alcove. Rhodamine WT is recommended for use as a water tracer (*Smart and Laidlaw*, 1977) and is assumed to be conservative, especially in surface flows, but there are issues with sorption to organics (*Soerens and Sabatini*, 1994). Results from the tracer test were used for modeling the alcove flux and for estimating water velocities within the alcove. Breakthrough curves are shown in Appendix B.

2.2.2 Piezometers

PVC piezometers (3.175 cm inner diameter, ~ 1.22 m long) were pounded into the subsurface using a 1.5 m hollow steel tube, inner steel driving rod, and sledge hammer (Appendix A). Piezometers were positioned around the head of each alcove (Figures 2-4). The number and locations of piezometers was limited by the depth to the water table (> length of installation device in some cases) and ability to penetrate the substrate.

The piezometers were used to measure horizontal hydraulic gradients, water temperatures, and hydraulic conductivity (K). Hydraulic gradients were calculated by surveying the alcove surface water and the top of casing for each piezometer. The survey was performed using a total station (TOPCON GTS 223, Singapore). To determine hydraulic conductivity, slug tests were performed in each piezometer using a data logger and pressure transducer (Global Water Pressure Transducer, WL15X-015, Goldriver, CA, USA). Results were interpreted with the Bouwer-Rice method (Appendix A).

2.2.3 Water Temperature and Meteorological Data

Thermistors (Stowaway Tidbit Data Logger, Onset, Bourne, MA, USA), were tied to a string and lowered to the bottom of each piezometer to record subsurface water temperature. Water temperature readings were taken every 15 min continuously for approximately 10 days in August and September. These data were used to assign a temperature signal to each water inflow in the model.

Surface water temperatures were collected at the same time in the alcove. Multiple recorders were placed longitudinally from the head of each alcove to its mouth. The Norwood Slough site was deep enough to allow thermistors to record water temperatures at the bottom and middle of the water column. Thermistors were also placed in the main channel of the river next to the alcove. Recorded alcove water temperatures were used to compare to modeled alcove temperatures during model calibration.

During this same time period, air temperature was recorded at each alcove using air temperature probes (HOBO Data Logger, Onset, Bourne, MA, USA). Probes were ~2 m above the water surface at each site. The remaining meteorological data necessary for the model, solar radiation, wind speed and direction, and dew point temperature, were downloaded from an Agrimet station near Corvallis at the same elevation approximately 40 km away (*Reclamation*, 2007).

Features of each alcove and important locations such as piezometers and cold water upwellings were recorded with a GPS unit accurate to 1m (Pathfinder PRO XRS, Trimble, Sunnyvale, CA, USA).

2.3 Model Methods

2.3.1 Model

CE-QUAL-W2 "W2" (*Coles and Wells*, 2006) is a deterministic, 2D, longitudinal/vertical model that uses the finite difference method to solve the hydrodynamic (conservation of mass and momentum) and water quality (advection dispersion) equations. W2 is limited to surface water applications and cannot model surface/subsurface exchange; a process important in river systems, but negligible in this study due to the low slope of the alcoves. W2 is used in this study to maintain continuity with Willamette River studies using W2 by the ODEQ (*ODEQ*, 2006).

W2 predicts temperature by performing a dynamic energy balance on the stream to account for all sources and sinks of heat, and based on the solutions of the heat transport equation, (*Sinokrot and Stefan*, 1993; 1994):

$$\frac{\partial T}{\partial t} = \frac{1}{A}\frac{\partial}{\partial x}\left(AD\frac{\partial T}{\partial x}\right) - \frac{1}{A}\frac{\partial QT}{\partial x} + \frac{q_l}{A}\left(T_l - T\right) + \frac{H_w w}{c_w \rho_w A} + \frac{H_b p}{c_w \rho_w A} \qquad (1)$$

A = cross-sectional area of alcove, m^2; c_w = specific heat of water, J/(kg˚C); D = dispersion coefficient of alcove, m^2/s (Appendix A); H_b = heat flux into or out of alcove bed, W/m^2; H_w = heat flux into or out of alcove water surface,W/m^2; q_l = inflow per unit alcove length - hyporheic water, precip, anthropogenic inputs, $m^3/(s*m)$; Q = alcove flux, m^3/s; T_w = alcove water temperature, ˚C; T_l = temperature of lateral inputs - hyporheic water, precip., anthropogenic inputs, ˚C; p = wetted perimeter, m; w = width of stream, m; x, t = space & time coordinates, m, s; ρ_w = density of water, kg/m^3. The heat transport equation describes heat transport with advection-dispersion processes. Two variables in equation 1, H_b and H_w, each have separate equations dependent upon temperature and are

used in energy budget calculations (equations 3 and 4). Due to its complexity and nonlinearity the heat transport equation is solved numerically by W2.

The model grid for each alcove was constructed using bathymetric and GPS data. The model grid consists of segments along the alcove, and layers with depth. At Harrisburg Bar and Green Island the segments are approximately 40 m long and the layers are 0.1 m deep. The Norwood Slough segments are approximately 200 m long and layers are 0.2 m deep.

2.3.2 Description of Water Inflows to the Model

An alcove is a gaining system in the summer from both the bank and river. Water inflows to alcoves were modeled as multiple point sources and one distributed source. Water was input at an elevation of neutral density compared to the rest of the water column.

The total alcove flow, Q_{Total}, was measured by tracer test (Table 2). Q_{Total} is comprised of three different types of water inflows: Q_{DIST}, Q_{PREF}, and Q_{MS}; distributed, preferential, and mainstem, respectively (Figures 5-7). Q_{DIST} is a subsurface, distributed water inflow that is distributed based on each segment's surface area. Q_{PREF} is a subsurface, point source, water inflow that consists of multiple inflows each attached to a specific piezometer and location.

The unit flow rates (m^2/s) of Q_{DIST} and Q_{PREF} were each calculated using the Dupuit equation (*Todd and Davis*, 2005):

$$q = \frac{K\left(h_0^2 + h^2\right)}{2L} \quad (2)$$

where K = hydraulic conductivity, m/s; h_0 = upstream head, m; h = alcove head, m; L = flow path length, m.

Hydraulic conductivity throughout each alcove was not constant, (K values were higher at the head of the alcove and lower on the bank) meaning different unit flow rates were calculated using equation 2. The bank K value and corresponding unit flow rate was assigned to Q_{DIST}, and the higher, head of alcove K value and corresponding unit flow rate was assigned to Q_{PREF}. The two unit flow rates were multiplied by the length of corresponding alcove to compute their respective flow rates (m^3/s)

Q_{MS} is a surface, point source water inflow and only occurs at Harrisburg Bar where the mainstem of the Willamette flows over the head of the gravel bar and into the alcove. This flow rate was calculated by subtracting Q_{PREF} and Q_{DIST} from Q_{Total}.

Q_{Total} was greater than the calculated water inflow at all three sites. We believe this is due to inaccurate characterization of preferential subsurface flow not represented in the Dupuit equation, which assumes homogeneous conditions. Due to the difficulty in characterizing these flow rates, Q_{PREF} was assigned the remaining inflow needed to meet the discrepancy and equal the outflow rate, Q_{Total}. All inflows have a constant flow rate for the 10 day model simulation.

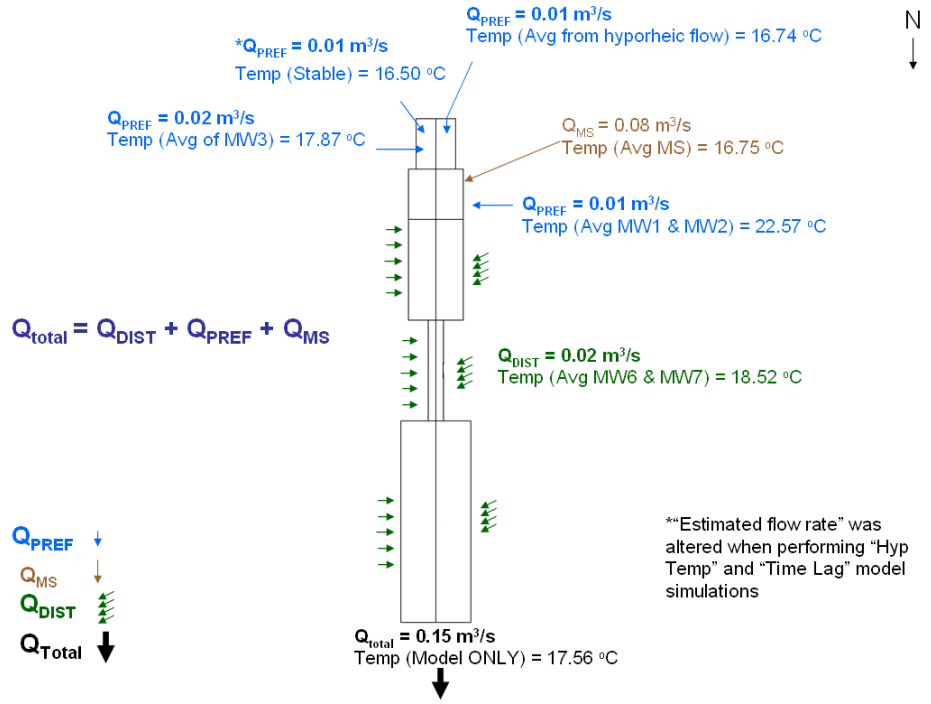

Figure 5. Harrisburg Bar; quantities and temperatures of inflows.

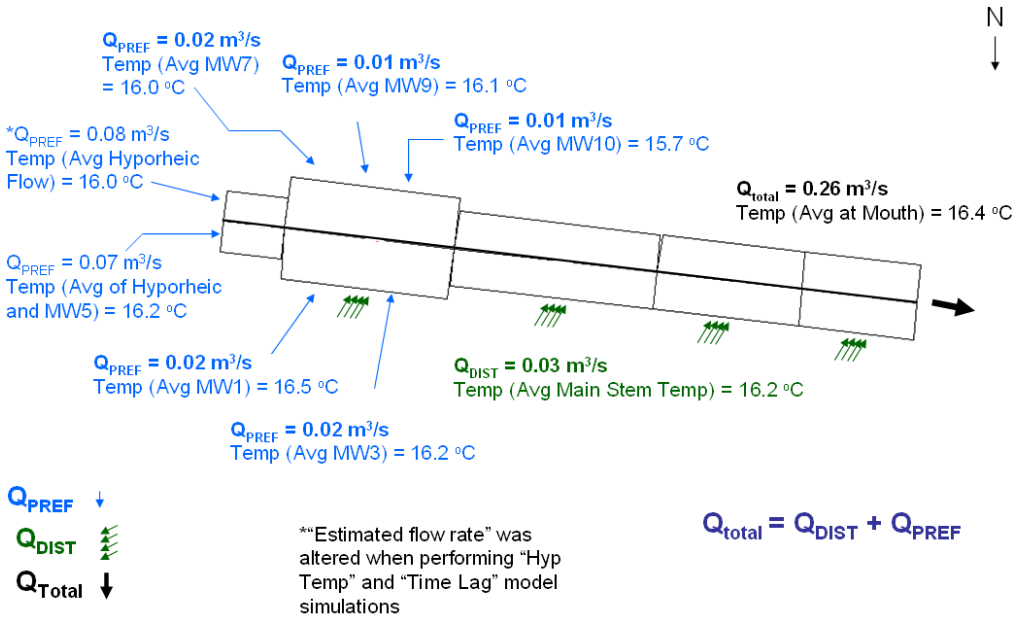

Figure 6. Green Island; quantities and temperature of inflows.

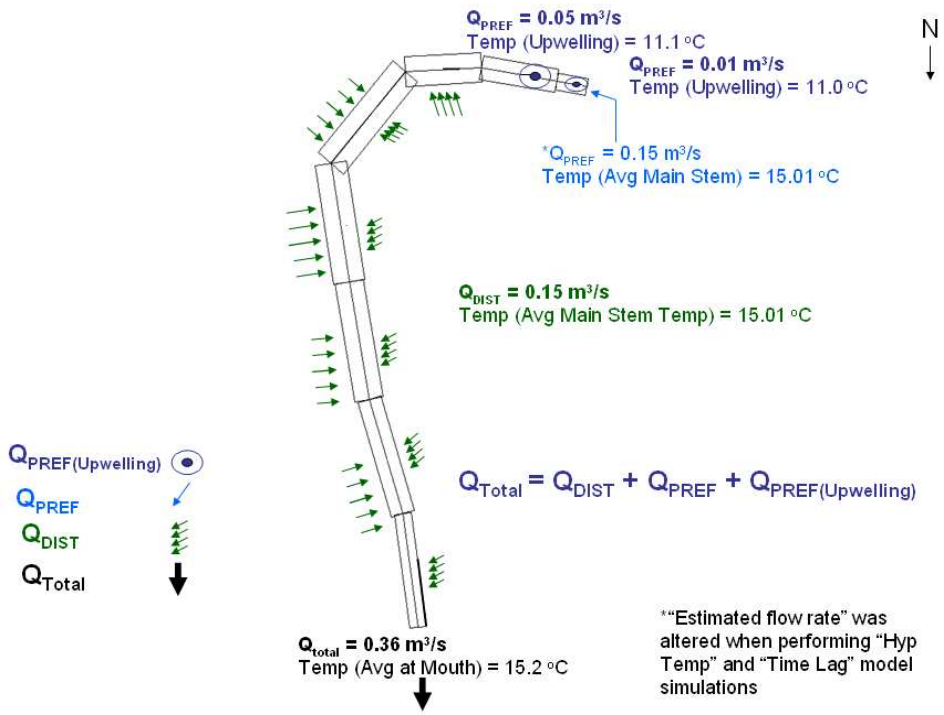

Figure 7. Norwood Slough; quantities and temperature of inflows.

2.3.3 Description of Temperature Inflows to the Model

The three water inflows, Q_{DIST}, Q_{PREF}, and Q_{MS}, each have a different temperature signal. Q_{DIST} has a corresponding temperature signal that is either an average of multiple thermistors (MW6 & MW7, Harrisburg Bar), or is an average of the mainstem temperature signal (Green Island and Norwood Slough). Q_{PREF} is divided into multiple point source inflows, and each inflow has a corresponding temperature signal from a specific thermistor in a piezometer. $Q_{MS,}$ has a corresponding temperature signal from the mainstem near Harrisburg Bar.

The temperature signal attributed to most inflows is variable. Thermistors recorded a water temperature every 15 min for 10 days. The "added" portion of Q_{PREF} that was needed to meet the Q_{Total} discrepancy was assigned a static inflow temperature approximately equal to the average temperature of the nearest thermistor in a piezometer.

2.3.4 Sources and Sinks

Heat sources and sinks in each alcove were calculated deterministically, which required substantial data inputs. Data required for performing an energy balance at the alcove water surface were as follows: incoming solar radiation, air temperature, dew point temperature, wind speed and direction, and cloud cover. To calculate the energy balance at the alcove's water surface the following equation can be used (*Coles and Wells*, 2006):

$$H_w = H_s + H_a + H_e + H_c - \left(H_{sr} + H_{ar} + H_{br}\right) \quad (3)$$

where H_w = heat flux into or out of alcove water surface, W/m^2; H_s = incident shortwave solar radiation, W/m^2; H_a = incident long wave radiation, W/m^2; H_e = evaporative heat loss, W/m^2; H_c = heat conduction, W/m^2; H_{sr} = reflected short wave solar radiation, W/m^2; H_{ar} = reflected long wave radiation, W/m^2; H_{br} = back radiation from alcove water surface, W/m^2. H_{br}, H_e, and H_c require additional equations to compute and are referenced in the W2 manual (*Coles and Wells*, 2006; *Cox and Bolte*, 2007).

The energy balance at the alcove bed is given by the first order approximation, Newton's law of cooling (*Coles and Wells*, 2006):

$$H_b = -K_{sw}\left(T_w - T_s\right) \quad (4)$$

where H_b = heat flux into or out of alcove at bed surface, W/m^2; K_{sw} = coefficient of sediment/water heat exchange, W/(m^2 ^{o}C); T_w = water temperature, ^{o}C; T_s = sediment temperature, ^{o}C.

Dynamic shading accounted for vegetative and topographic shading of the alcove's water surface, with respect to daily and seasonal location of the sun and foliage.

2.3.5 Calibration

Thermal calibration of the model was achieved by manually varying 8 parameters (Table 4). Calibration was carried out by minimizing the Mean Absolute Error (MAE) and Root Mean Squared Error (RMSE) between the modeled and observed data (Table 3). Due to the short time frame (10 days) over which data were collected, a validation run could not be performed because all data were used for calibration.

The division of Q_{PREF} into multiple point source inflows, and assignment to their corresponding temperature signals was based on the combination that provided the best calibration and lowest RMSE (*Loheide and Gorelick*, 2006). A specific temperature signal was assigned to each input was done to increase the thermal resolution of the model, which critically influences model results since cool patches in alcoves are highly localized and potentially dependant on location specific inputs and their corresponding temperature (*Ebersole et al.*, 2003b).

2.4 Sensitivity Analysis

A sensitivity analysis was performed to determine how sensitive the model outputs are to changes in parameter values. The sensitivity analysis was performed using three approaches: the Temperature Sensitivity Index (TSI), Max ΔT_{max} and the Projected Alcove Temperature.

2.4.1 Temperature Sensitivity Index (TSI)

The TSI is twice the fraction of variability in the maximum alcove temperature attributable to a parameter. It is a measure of the importance of a parameter to the

existence of CWR (and other cool patches) in alcoves on the Willamette River. The TSI is calculated using the following equation:

$$TSI = \left| \frac{\Delta T_{\max}}{\Delta Param} \times \frac{Param\_range}{T\_range} \right| \quad (4)$$

The TSI makes possible the comparison of different parameters' effects on the temperature of all alcoves, such as shade and hyporheic temperature. Similar parameters have been used to examine the contribution of parameter uncertainty to uncertainty in model results (*Harvey et al.*, 1996). ΔT_{max} is the amount of change in the seven day average of the maximum daily temperature (SDAMDT) [^{o}C] due to a change in the value of a parameter, $\Delta Param$ [various units]. So that different parameters are comparable, this ratio is normalized to the local range of each parameter, *Param_range* [various units]. This is the difference between the maximum and minimum values of the parameter that could realistically occur on the Willamette River in the summer. For example, the hyporheic inflow temperature has a range of 11-24 ^{o}C at the 3 alcoves. If we stopped here, the TSI number would have units of ^{o}C and would compare, for example, the effect of changing shade to the effect of changing hyporheic temperature. To compare alcoves, normalization of ΔT_{max} is also required because each alcove has a different temperature relationship with the mainstem. For example, a 0.5 ^{o}C temperature change due to the change in a given parameter (e.g., a 20% change in shade) would be more significant at Harrisburg Bar than at Green Island because the alcove water temperature at Harrisburg Bar is very close to the mainstem temperature. Thus, we normalize with the other alcoves on the Willamette using *T_range*, which is the difference between the alcove temperature

and the mainstem temperature at the time of the mainstem maximum temperature, averaged over seven days.

The value of the TSI indicates the parameter's importance to alcove temperature. When ΔT_{max} is equal to *T_range* it produces a TSI of approximately 2. This is because the maximum ΔParam is approximately 1/2 of *Param_range*. If ΔT_{max} equals *T_range* then *ΔParam* could generate 100% of the observed difference between the alcove and mainstem. Thus, parameters with a TSI equal or greater than 2 are very important to the alcove's temperature, while a TSI much less than 2 means the parameter is less important.

The TSI was calculated 3 times for every parameter and then averaged (Table 4). Each parameter was assigned three different values: minimum, half way between minimum and maximum (nominal median), and maximum parameter value. Minimum and maximum values are unlikely (e.g., 100% shade over an alcove is unlikely), but since the model responses are generally nonlinear functions of parameters, the extremes were used to capture the entire range of possible outcomes produced by the parameters. Most calibrated parameters had values close to the nominal median, which allowed for the comparison of the model's response to both large and small changes in the parameter value. The TSI was not calculated for the 'lag time' parameter due to the temperature variation (+/-) for different time lags.

2.4.2 Max ΔT_{max}

The *Max* ΔT_{max} is the greatest change in SDAMDT that can be produced in an alcove by altering a parameter to its most extreme value. For example, at Norwood

Slough a parameter value of 100% shade could decrease the alcove SDAMDT by 2.2 ^{o}C. *Max* ΔT_{max} is reported as absolute value.

2.4.3 Projected Alcove Temperature

The SDAMDT was evaluated for a complete range of values for 4 parameters. The resulting graphs display alcove SDAMDT with respect to the range of possible parameter values.

Subsurface travel time across the gravel bar ("lag time") was not measured in the field and was evaluated in this context. The solution for steady one-dimensional fluid flow in a semi-infinite porous medium with sinusoidal surface temperature (*Stallman*, 1965), modified for horizontal movement through the subsurface with longitudinal dispersion is

$$T - T_A = \Delta T e^{-az} \times \sin(2\pi t / \tau - bx) \quad (5)$$

where T = temperature at any point x, t, ^{o}C; T_A = average ambient temperature at the land surface, ^{o}C; ΔT = amplitude of the temperature variation at the surface, ^{o}C; $a = ((U^2+V^4/4)^{1/2}+V^2/2)^{1/2}-V$; $b = ((U^2+V^4/4)^{1/2}-V^2/2)^{1/2}$; t = time, s; v = velocity of water along the flow path, cm/s; x = depth below the land surface, cm; τ = period of oscillation of temperature at land surface, s (U and V are coefficients containing advection and dispersion information and are defined in Appendix A). Using equation 5 and the temperature signal from the mainstem above the alcove; a 10-day subsurface temperature signal was calculated for lag times ranging from 1 hour to 1 month. The calculated temperature signal was then input into the model to determine how the hyporheic lag time would affect the alcove temperature.

3. RESULTS

3.1 Thermistor Results

The location in and around the alcove determined the amplitude of the diurnal temperature signal. Thermistors recording temperature in the alcove had greater diurnal amplitude than thermistors placed in piezometers (Figure 8). The amount of diurnal amplitude also varied depending on the location within the alcove. Thermistors located near the head of the alcove and close to emerging hyporheic flow had smaller amplitude than thermistors near the mouth of the alcove or in the mainstem. In addition, thermistors located in the middle of the water column (RW034 Norwood Slough, Figure 8c), had the greatest amplitude of all thermistors.

The location in the alcove also determined the time lag of the temperature signal. Thermistors located at the head of the alcove recorded a maximum daily temperature either before (Figure 8b) or after (Figure 8a, c) the mainstem maximum daily temperature. The time lag between these thermistors and the mainstem thermistor ranged from 2 to 12 hours. The same phenomenon also occurred for the daily minimum temperatures. The period of the temperature signal converged with that of the mainstem for thermistors close to the mouth of the alcove. MW2 at Harrisburg Bar was the only piezometer that had enough amplitude to show a time lag, which was 12 hours.

The warmest temperatures were recorded at Harrisburg Bar and coolest at Norwood Slough, (Figure 8a, c). Piezometers MW1 and MW2, located on an unvegetated gravel bar, recorded temperatures that averaged 5.75 ^{o}C warmer than the hyporheic flow emerging into the head of the alcove (A12). At Norwood Slough, thermistors in cold water upwellings recorded steady temperature signals that were 4 ^{o}C cooler than the

mainstem average temperature. Due to the depth of the water column and cold water at Norwood Slough, stratification is occurring in the alcove. Green Island had the narrowest observed temperature range in both the alcove and piezometers (Figure 8b).

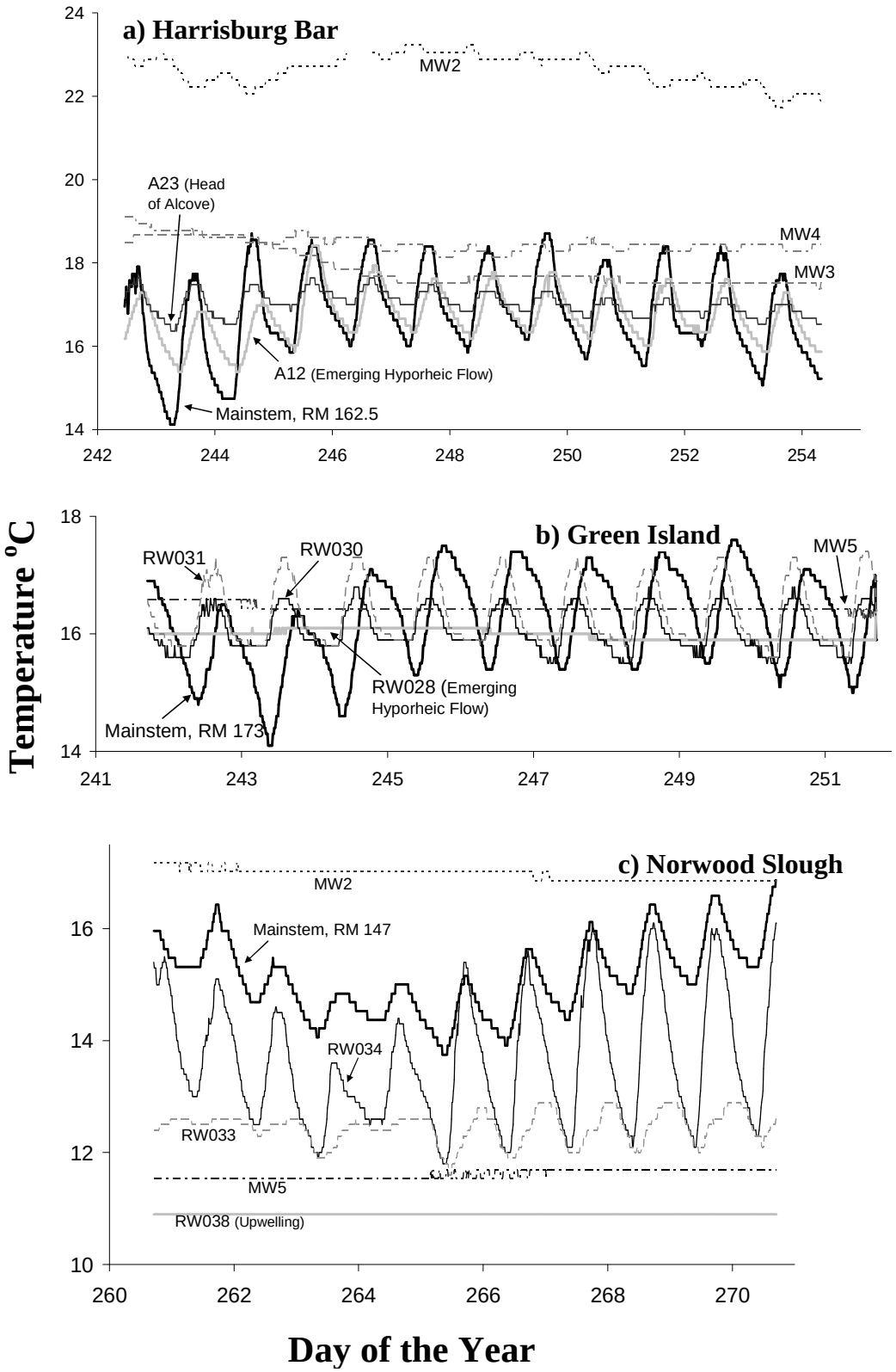

Figure 8. Thermistor data.
Thermistors placed in piezometers around the alcove are labeled as MW#. Thermistors placed directly in the alcove are labeled as A# or RW#.

3.2 Model Results

Modeled alcove temperatures were compared to observed temperatures for every thermistor location in the alcoves (Figure 9, Appendix C). Thermistors located at the head of the alcoves, Harrisburg Bar-A23, Green Island-RW030, and Norwood Slough-RW036, were located in the most important sites for CWR and so were weighted more heavily to calibrate their respective models, evident by the low RMSE values at the head of each alcove (Table 3).

Comparison of modeled to observed alcove temperatures reveals some of the difficulties encountered in the modeling process (Figure 9). The period of the modeled temperatures is unintentionally lagged at Norwood Slough. The amplitude of the temperature signal is incorrect at Harrisburg Bar. Different combinations of realistic parameter values did not cause the models to perfectly represent the observed temperatures.

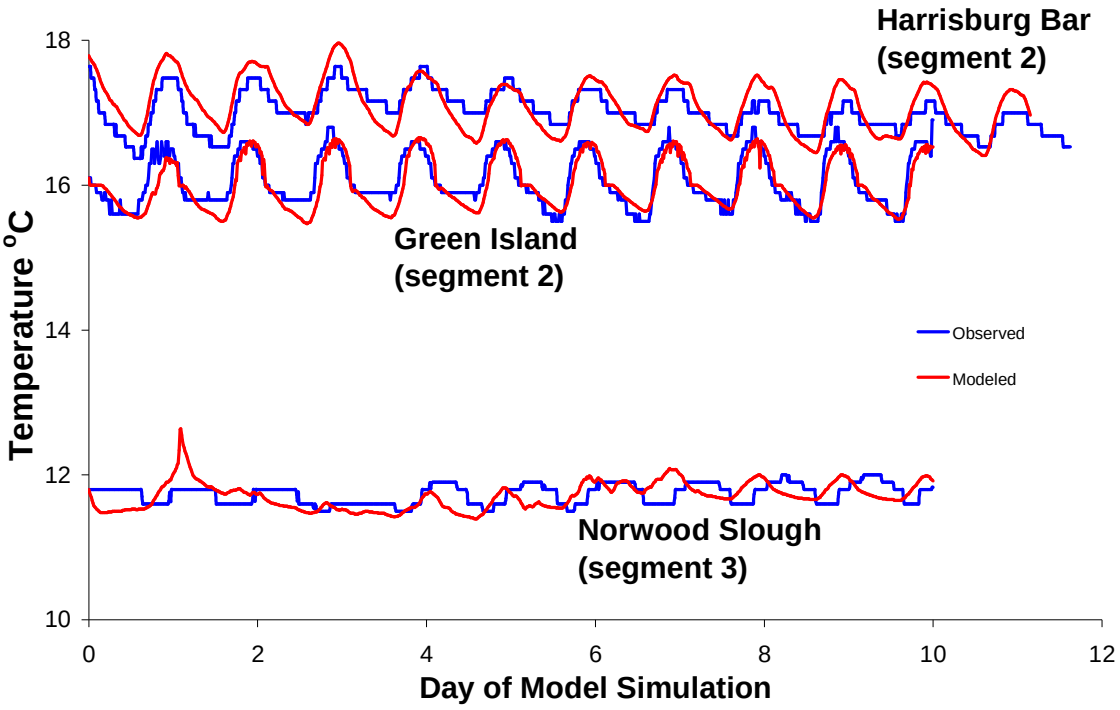

Figure 9. Comparison of modeled vs. observed temperature at head of alcove.

Table 3. Results of model calibration.

	Model Segment	Number of Data	MAE, °C	RMSE, °C
Harrisburg Bar	2	1187	0.20	0.23
	Model Segment	**Number of Data**	**MAE, °C**	**RMSE, °C**
Green Island	2	1000	0.15	0.19
	3	1000	0.30	0.41
	4	1000	0.28	0.64
	5	1000	0.37	0.53
	6	1000	0.37	0.44
	Model Segment	**Number of Data**	**MAE, °C**	**RMSE, °C**
Norwood Slough	3	1000	0.18	0.21
	4 mid	1000	0.95	1.11
	4 bottom	1000	0.94	1.09
	5 mid	1000	0.81	0.96
	5 bottom	1000	0.55	0.68
	6 mid	1000	0.74	0.87
	6 bottom	1000	1.20	1.46
	7 mid	1000	0.89	1.01
	7 bottom	1000	0.87	1.00
	9	1000	1.16	1.56

3.3 Sensitivity Analysis

3.3.1 Temperature Sensitivity Index

Values for the TSI ranged between 0.0 and 4.0 for all sites, with the exception of Green Island that had one value of 9.9, (Table 4, Figure 10). Hyporheic temperature was the only parameter at Harrisburg Bar and Green Island to have a TSI greater than 2.0, indicating it was the only parameter to which the alcove temperature was very sensitive. Green Island, was more sensitive to cooler (11-15.0 ^{o}C) hyporheic temperature than warmer (15.5-18 ^{o}C). Norwood Slough had TSI values greater than 2.0 for wind, shade, and hyporheic temperature, indicating it was sensitive to multiple parameters.

Max ΔT_{max} values are generally consistent with the TSI, but the most extreme possible parameters re-order some relative magnitudes (Figure 10). The percent of solar radiation reflected by the sediment back into the water column (TSEDF) has the potential

to increase Harrisburg Bar's temperature 0.85 ^{o}C, due to the alcove's shallow, unshaded geometry. Likewise, Norwood Slough's alcove temperature could decrease by 2.24 ^{o}C if 100% of the wind were to reach the alcove instead of some fraction being blocked by trees, because the alcove is large and deep.

Table 4. Sensitivity analysis.

	Parameter	Avg TSI	Max ΔT_{max} ^{o}C
Harrisburg Bar	Wind Sheltering Coefficient (WSC)	0.00	0.00
	Light Extinction from Water (EXH2O)	-0.01	0.03
	Coefficient of Bottom Heat Exchange (CBHE)	0.01	0.01
	Alcove Flux (AF)	0.06	0.10
	Shade	0.13	0.15
	Solar Radiation Absorbed at Surface (BETA)	0.23	0.17
	Sediment Reflection of Solar Radiation (TSEDF)	0.70	0.85
	Hyporheic Temperature (HT) @ 11 ^{o}C	2.42	1.44
	Hyporheic Temperature (HT) @ 18 ^{o}C	2.42	1.89
	Parameter	**Avg TSI**	**Max ΔT_{max} ^{o}C**
Green Island	Wind Sheltering Coefficient (WSC)	0.00	0.00
	Light Extinction from Water (EXH2O)	0.06	0.04
	Coefficient of Bottom Heat Exchange (CBHE)	0.00	0.00
	Alcove Flux (AF)	0.08	0.32
	Shade	0.94	0.80
	Solar Radiation Absorbed at Surface (BETA)	0.28	0.18
	Sediment Reflection of Solar Radiation (TSEDF)	0.24	0.11
	Hyporheic Temperature (HT) @ 11 ^{o}C	9.90	5.59
	Hyporheic Temperature (HT) @ 18 ^{o}C	3.93	1.49
	Parameter	**Avg TSI**	**Max ΔT_{max} ^{o}C**
Norwood Slough	Wind Sheltering Coefficient (WSC)	2.49	2.24
	Light Extinction from Water (EXH2O)	0.84	0.44
	Coefficient of Bottom Heat Exchange (CBHE)	0.15	0.07
	Alcove Flux (AF)	1.21	0.42
	Shade	3.82	2.24
	Solar Radiation Absorbed at Surface (BETA)	0.23	0.05
	Sediment Reflection of Solar Radiation (TSEDF)	1.10	0.33
	Hyporheic Temperature (HT) @ 11 ^{o}C	3.43	1.70
	Hyporheic Temperature (HT) @ 18 ^{o}C	3.43	1.02

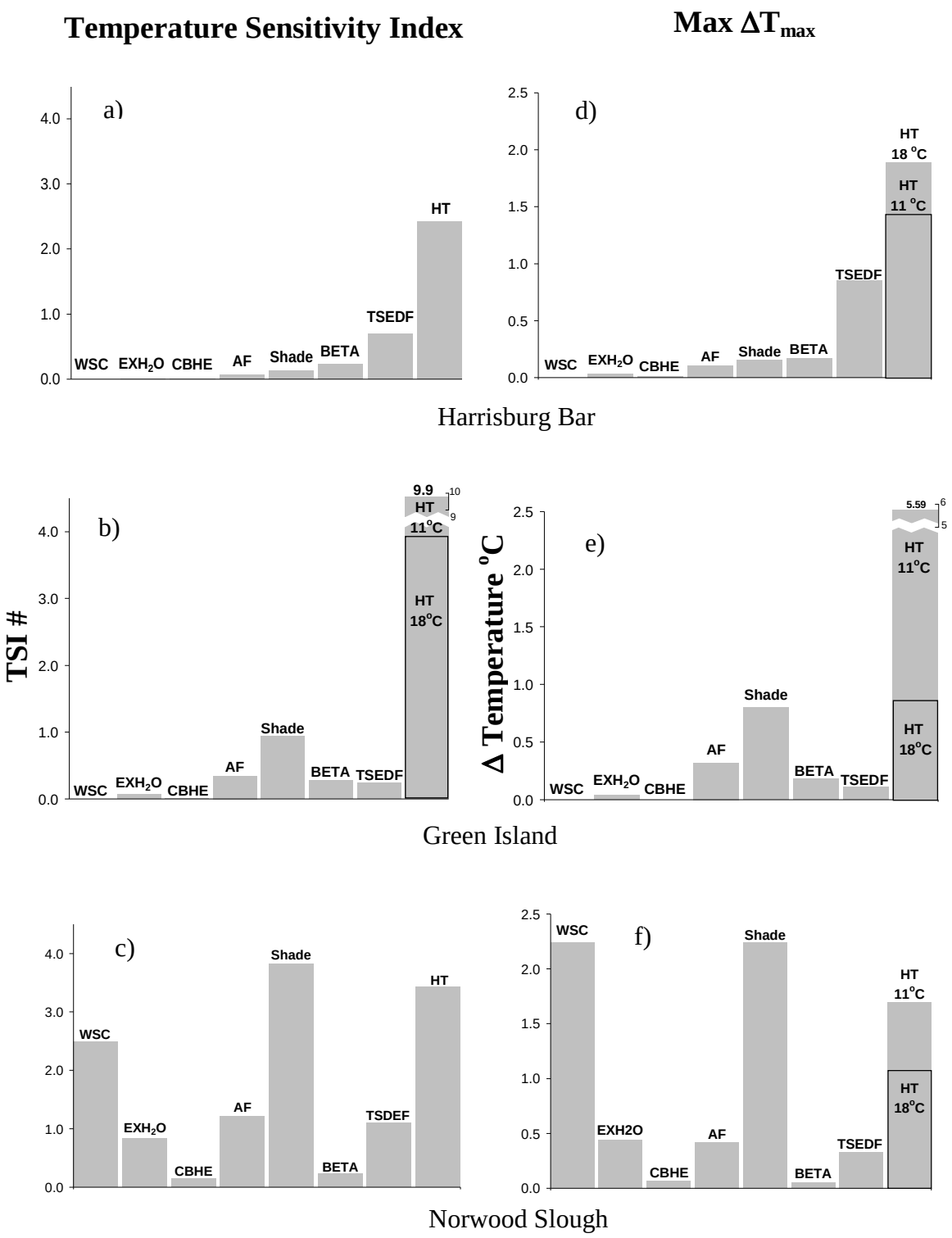

Figure 10. Temperature Sensitivity Index (a,b,c) and Max ΔT_{max} (d,e,f). Harrisburg Bar, Green Island, and Norwood Slough were calibrated with hyporheic inflows of 16.5, 16.0, and 15.0 ^{o}C respectively.

3.3.2 Projected Alcove Temperature

The Projected Alcove Temperature is the range of possible SDAMDT responses of each alcove when modeled with a range of values. Four parameters were investigated: hyporheic temperature, shade, alcove flux, and lag time of hyporheic flow. All of the four parameters are shown for Harrisburg Bar (Figure 11). For comparison, the lag time parameter is shown for all 3 alcoves (Figure 12). The remaining figures can be found in Appendix D.

Increasing the temperature of the hyporheic flow at Harrisburg Bar (Figure 11a) causes a 3.31 ^{o}C increase in alcove temperature over a hyporheic inflow temperature range of 11-24 ^{o}C. Increasing the amount of shade (Figure 11b) at Harrisburg Bar decreases the SDAMDT by 0.19 ^{o}C over the 100% range of shade values.

Increasing the flux of water through the alcove moves the alcove temperature toward the average temperature of the inflowing water (Figure 11c). Variations in Projected Alcove Temperature for fluxes less than 100% of Q_{Total} are suspect because most alcoves have a constant source of water moving through them. This advection in the alcove prevents water from stagnating. Lentic water is subject to much different conditions than moving water and thus, the water temperature of the alcove is more sensitive to all of the model parameters at fluxes less than 100% of Q_{Total}.

The lag time for hyporheic flow has a sinusoidal pattern with decreasing amplitude (Figure 11d). The lag time of hyporheic flow can cause either higher or lower average alcove temperatures depending on the time of day it enters the alcove (Figure 12a, b, c).

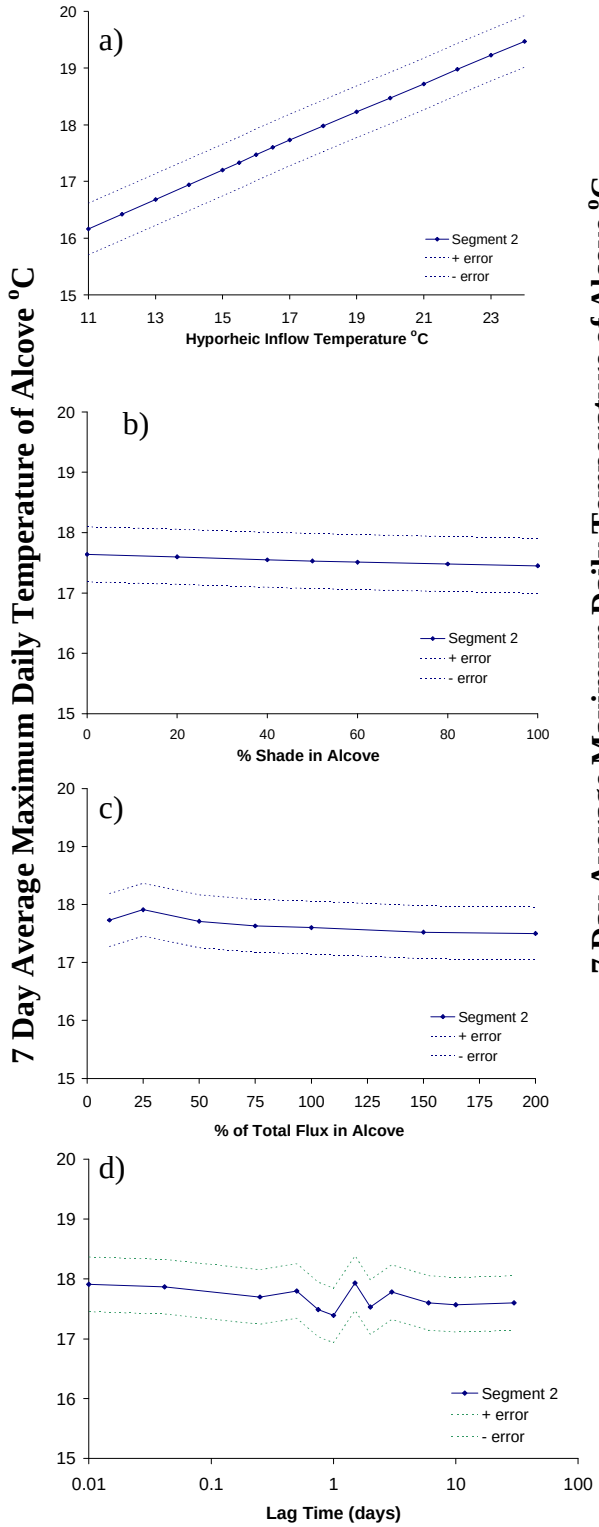

Figure 11. Projected Alcove Temperature for Harrisburg Bar.

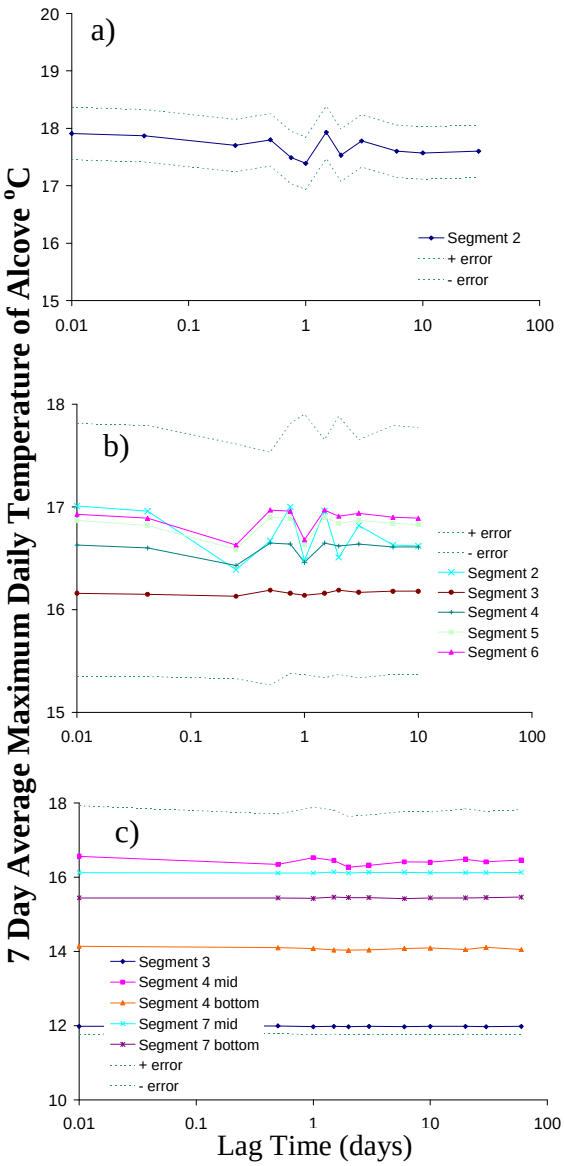

Figure 12. Projected Alcove Temperature, Time Lag. a)Harrisburg Bar, b) Green Island, c) Norwood Slough.

4. DISCUSSION

4.1 Alcove Size and Residence Time

The size and hydraulic residence time of an alcove are important factors in determining the main drivers of alcove temperature. A large alcove (e.g., Norwood Slough) often has water with a long hydraulic residence time, (c.f., Table 2) so that it behaves more like a lentic system, meaning meteorological conditions drive alcove temperature. Large alcoves have a long fetch, meaning they are susceptible to the effects of wind (i.e., mixing and evaporation) (Figure 10c, f).

Shade, which can significantly reduce the solar radiation reaching the alcove (*Ebersole et al.*, 2003b; *Johnson*, 2004), had a greater impact on large alcoves, in this study, because the alcove water is exposed to the sun for a longer period of time (Figure 10c, f). Research also shows that some very small alcoves (~20 m) with long hydraulic residence times and are impacted by shade (*Ebersole et al.*, 2003b), suggesting that an alcove's hydraulic residence time determines the effect of shade more than the alcove's size.

Small alcoves with short hydraulic residence times, such as Harrisburg Bar and Green Island, have temperatures dominated by the temperature and flux of subsurface water emerging into the alcove (Figure 10a, b, d, e; Figure 11a). Hydraulic residence times in the small alcove are too short (Table 1) for meteorological conditions to significantly affect the alcove's water temperature (Figure 10a, b, d, e). Advection is more important than heat sources and sinks and thus advection dominates the alcove's thermal regime. Many alcoves on the Upper Willamette River are similar in size to Harrisburg Bar and Green Island (Landers, D., unpublished data), and therefore the

remainder of this discussion will focus on factors most important to small alcove temperature.

4.2 Alcove Flux

Alcove flux, along with alcove size, determines residence time which strongly influences meteorological impact. Alcoves become less affected by meteorological conditions and more by the temperature of the incoming water as alcove flux increases. The SDAMDT of the 3 alcoves converged on their average input temperature as alcove flux increased (Figure 11c, Appendix D). Alcove flux was not indicated by the TSI as an important parameter (value << 2) because it has an indirect affect on alcove water temperature. A higher alcove flux reduces alcove residence time and buffers the alcove from diurnal meteorological conditions thereby creating a stable temperature regime (Figure 11c) (*Loheide and Gorelick*, 2006; *Poole and Berman*, 2001).

Alcove flux is controlled by the hydraulic gradient and hydraulic conductivity of the gravel bar as described by Darcy's Law, $Q = -KA(dh/dl)$ (*Todd and Davis*, 2005). Increasing either the gradient or the hydraulic conductivity (*K*) will increase the discharge of water into the alcove.

4.3 Hyporheic Lag Time

Recent research has speculated on potential methods of 'hyporheic cooling' (*Fernald et al.*, 2006; *Story et al.*, 2003), but has not been able to delineate and quantify the processes. It may be helpful to delineate three different thermal zones that describe the fluctuations of subsurface temperature. The diurnal zone, along short hyporheic flow paths, contains water with residence times less than several days, and has fluctuations in

temperature dominated by daily changes in air temperature. The seasonal zone, along intermediate-length hyporheic flow paths, contains water with residence times of months, and has seasonal fluctuations but not diurnal (*Silliman and Booth*, 1993). The average temperature in the seasonal zone is approximately equal to the average seasonal temperature of surface water (*Malard et al.*, 2001; *Peterson and Sickbert*, 2006; *Taniguchi*, 1993). The steady-state zone, along deep and lengthy hyporheic or groundwater flow paths, contains water with residence times of years, has very little temperature fluctuation, and can be considered constant for the purposes of this study (*Anderson*, 2005). Water temperatures in the steady-state zone are approximately the same temperature as the mean annual air temperature (*Domenico and Schwartz*, 1990).

The temperature of hyporheic water is determined by the subsurface residence time or "lag time." The length of lag time determines the temperature at which the hyporheic water will emerge into the alcove. Hyporheic water is moving slower than the mainstem, with subsurface residence times of 0.2 to 30 hours for major flow paths in the main channel on the Willamette River (*Fernald et al.*, 2001). However, lag times can vary between hours and years (particularly for groundwater), and the longer lag times reduce temperature fluctuations due to dispersion (Figure 13) (*Stallman*, 1965).

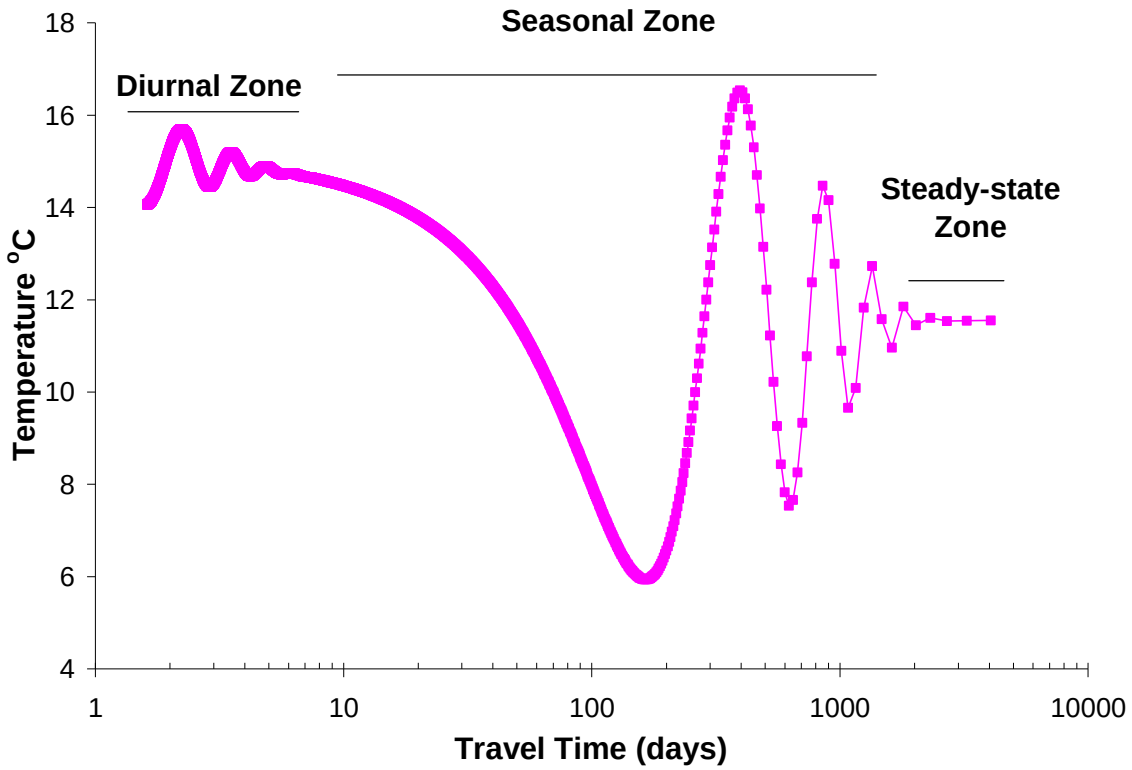

Figure 11. Theoretical temperature dispersion due to lag time of subsurface flow.

Lag times are affected by the hydraulic conductivity, size, and hydraulic gradient of the gravel bar. In this study and another (*Burkholder,* 2007), thermistors located near the diurnal zone recorded temperature signals with varying degrees of diurnal and seasonal fluctuation indicating a wide range of lag times (Figure 8).

4.3.1 Lag Time: Hour to Days

Hyporheic flow with a subsurface lag time of hours to days still retains most of its diurnal temperature signal when it emerges into the alcove. Only one of the thermistors in a piezometer, MW2 at Harrisburg Bar, had diurnal fluctuation in its temperature signal (Figure 8a). At hourly to daily lag times the average temperature of the hyporheic flow emerging into the alcove will not be colder than the average temperature of the mainstem, if there are no other influences on the hyporheic water. Simply, the emerging hyporheic

flow is out of phase with the surface water, causing destructive interference with the temperature of the alcove.

Models of Harrisburg Bar and Green Island (Figure 12a, b), show a decreasing fluctuation in the SDAMDT as the lag time increases. This is because the diurnal temperature signal of the emerging hyporheic flow is decreasing along with the potential for destructive interference. The results from the Harrisburg Bar and Green Island Sites (Figure 12a, b), also show a maximum decrease in SDAMDT at a 1-day time lag. This is incorrect, and can be attributed to an incorrect estimate in the flow path length, but the concept remains valid.

4.3.2 Lag Time: Tens of Days to Seasonal

Hyporheic flow with a subsurface lag time of tens of days has no diurnal temperature signal, and is approximately the same average temperature as the mainstem (MW5 in Figure 8b). These lag times are beneficial in regulating the alcove water temperature because of the buffering affect of a constant source of stable water temperature (*Poole and Berman*, 2001). Hyporheic flow with a subsurface lag time spanning a season will have a different average temperature than that of the mainstem. Monthly average temperatures on the Willamette, at Harrisburg, OR (RM 161) are 5.5 degrees cooler in May than July (USGS, 2007).

4.3.3 Lag Time: Years

Hyporheic flow with a subsurface lag time of years disperses its seasonal temperature signal, thereby moving into equilibrium with the mean annual air temperature. This is the coldest temperature that subsurface water can achieve and

therefore the most beneficial to alcove temperature with respect to mitigating maximum daily temperatures in the late summer.

Cold water upwellings measured at Norwood Slough indicate a lag time of years (Figure 8c). At this point, the subsurface water has reached the same temperature as the groundwater, yet if it originated in the mainstem it is still classified as hyporheic water (*Bencala*, 2005). However, without performing isotopic analyses it is difficult to distinguish hyporheic water from groundwater at extended time lags.

4.4 River Geomorphology and Floodplain Restoration

The movement of hyporheic water through the subsurface is dependent upon channel sinuosity, floodplain structure and composition, hydraulic gradients, hydraulic conductivity, the heterogeneity of the channel, and bed forms (*Boano et al.*, 2006; *Cardenas et al.*, 2004; *Kasahara and Wondzell*, 2003). Point bars are a type of bed form particularly conducive to hyporheic flow. On some rivers, point bars often contain alcoves on their downstream end, which receive the hyporheic flow moving through the gravel bar. This hyporheic flow can be the main contributor of water to the alcove (Figure 3) (*Fernald et al.*, 2006).

The creation and maintenance of geomorphic features (e.g., point bars) is dependent upon the flow regime in a river system. These features are unstable with respect to bed load movement and are susceptible to alteration in a dynamic river system (*Fowler and Death*, 2001). For example, gravel bars migrate across the river channel (*Dykaar and Wigington*, 2000), and meander bends move forming oxbows or point bars (*Leopold et al.*, 1964). These processes, crucial for alcove formation, occur at bankfull discharge when the river has enough energy to move its bed load (*Poff et al.*, 1997).

In addition to creating and maintaining channel features, bed load movement counteracts the affects of colmation (*Brunke and Gonser*, 1997). This clogging of hyporheic interstices by fine particles lowers the hydraulic conductivity of the hyporheic zone reducing the flux of hyporheic water into the alcove (*Fernald et al.*, 2006). The effects of colmation can be seen at the 3 study sites. Harrisburg Bar, the youngest studied site with the least colmation, had the highest hydraulic conductivity and greatest diurnal fluctuation in its subsurface temperature signal (MW2 Figure 8a). Green Island, the middle aged site with moderate colmation, had a lower hydraulic conductivity and no diurnal temperature signal (MW5 Figure 8b). Norwood Slough, the oldest studied site, had the most colmation evident by the lowest hydraulic conductivity and cold water upwellings-which indicate long subsurface residence times RW038 Figure 8c). Thus, long subsurface residence times generate cooler upwelling water, but lower hydraulic conductivity substantially reduces subsurface flow. Likewise, short subsurface residence times and high hydraulic conductivity produce more, but slightly warmer, subsurface flow.

An increase in alcove population and CWR, which are dependent on channel bedform and riparian features (*Ebersole et al.*, 2003a), could occur through floodplain restoration practices. The formation of geomorphic features requires bankfull flows and access to sediment. Anthropogenic structures (i.e., bank hardening and dams) prevent access to sediment via channel migration (*Poff et al.*, 1997). Removal of bank hardening structures and reconnection of side channels will allow the river to access its new sediment sources, increase habitat heterogeneity, and create new bed forms conducive to

high hyporheic flow rates (*Fernald et al.*, 2001; *Fernald et al.*, 2006; *Poff et al.*, 1997; *Poole and Berman*, 2001).

The effects of bank hardening can be seen along the lower reach of the Willamette River where the river is composed almost entirely of the main channel and has very few alcoves, side channels, or islands. In comparison, the upper reach of the Willamette River, which is the least the constrained, has more alcoves, side channels, and islands (*Hulse et al.*, 2002). The upper reach, which contains all 3 study sites, still has the ability to create and maintain new channel forms as is evident by the recent formation of Harrisburg Bar.

5. CONCLUSION

Three alcoves on the Willamette River were studied to determine the processes influencing their temperature. It was found that alcoves of different sizes have different flow rates and vary in their response to meteorological conditions. Large alcoves with low flux are most sensitive to meteorological conditions. Small alcoves with high flux rates are more sensitive to the temperature of emerging subsurface flow than to meteorological conditions.

The temperature of emerging hyporheic flow is determined by its residence time in the subsurface. Hyporheic flow retains its diurnal temperature signal for residence times of hours to days. Hyporheic flow disperses its diurnal temperature signal and moves into equilibrium (either seasonal or annual) for extended residence times. Areas potentially important to alcove temperature that were not covered in the scope of this study are alcove volume and surface area.

Off Channel Habitat and Cold Water Refugia cannot exist without channel complexity. Alcoves require bankfull flow and accessible sediment for their formation and maintenance. Thus, floodplain restoration must focus on environmental flows and removal of bank hardening structures. Multiple benefits that can be gained through the holistic approach of floodplain restoration must be considered when comparing it to engineered solutions.

References

Anderson, M. (2005), Heat as a ground water tracer, *GROUND WATER*, *43*(6), 951-968.

Arscott, D., et al. (2001), Thermal heterogeneity along a braided floodplain river (Tagliamento River, northeastern Italy), *CANADIAN JOURNAL OF FISHERIES AND AQUATIC SCIENCES*, 2359-2373.

Bencala, K. E. (2005), Hyporheic Exchange Flows, in *Encyclopedia of Hydrological Sciences*, edited by M. G. Anderson, John Wiley & Sons, Inc.

Boano, F., et al. (2006), Sinuosity-driven hyporheic exchange in meandering rivers, *GEOPHYSICAL RESEARCH LETTERS*, *33*(18), -.

Boulton, A., et al. (1998), The functional significance of the hyporheic zone in streams and rivers, *ANNUAL REVIEW OF ECOLOGY AND SYSTEMATICS*, *29*, 59-81.

Bouwer, H., and R. C. Rice (1976), Rice, A slug test for determining hydraulic conductivity of unconfined aquifers with completely or partially penetrating wells, *Water Resources Research*, *12*(3), 6.

Bouwer, H. (1989), The Bouwer and Rice slug test - an update., *Ground Water*, *27*(3), 6.

Brown, G. W. (1969), Predicting Temperature of Small Streams, *Water Resources Research*, *5*(1), 68-75.

Brunke, M., and T. Gonser (1997), The ecological significance of exchange processes between rivers and groundwater, *FRESHWATER BIOLOGY*, 1-33.

Burkholder, B. K. (2007), Influence of Hyporheic Flow and Geomorphology on Temperature of a Large, Gravel-bed River, Clackamas River, Oregon, USA, 170 pp, Oregon State University, Corvallis.

Caissie, D. (2006), The thermal regime of rivers: a review, *FRESHWATER BIOLOGY*, 1389-1406.

Cardenas, M., et al. (2004), Impact of heterogeneity, bed forms, and stream curvature on subchannel hyporheic exchange, *WATER RESOURCES RESEARCH*, *40*(8), -.

Coles, T., and S. Wells (2006), CE-QUAL-W2, edited, p. Hydrodynamic and Water Quality Model, Portland State University, Portland.

Cox, M., and J. Bolte (2007), A spatially explicit network-based model for estimating stream temperature distribution, *ENVIRONMENTAL MODELLING & SOFTWARE*, *22*(4), 502-514.

Domenico, P., and F. Schwartz (1990), *Physical and chemical hydrogeology*, Wiley, New York.

Dykaar, B., and P. Wigington (2000), Floodplain formation and cottonwood colonization patterns on the Willamette River, Oregon, USA, *ENVIRONMENTAL MANAGEMENT*, *25*(1), 87-104.

Ebersole, J., et al. (2003a), Thermal heterogeneity, stream channel morphology, and salmonid abundance in northeastern Oregon streams, *CANADIAN JOURNAL OF FISHERIES AND AQUATIC SCIENCES*, 1266-1280.

Ebersole, J., et al. (2003b), Cold water patches in warm streams: Physicochemical characteristics and the influence of shading, *JOURNAL OF THE AMERICAN WATER RESOURCES ASSOCIATION*, 355-368.

Evans, E., et al. (1998), River energy budgets with special reference to river bed processes, *HYDROLOGICAL PROCESSES*, 575-595.

Farthing, K. (2006), Investigation of the Temperature Impact of Hyporheic Flow: Using Groundwater and Heat Flow Modeling to Evaluate Temperature Mitigation Strategies on the Willamette River, Oregon, 107 pp, Oregon State University, Corvallis.

Fernald, A., et al. (2001), Transient storage and hyporheic flow along the Willamette River, Oregon: Field measurements and model estimates, *WATER RESOURCES RESEARCH*, 1681-1694.

Fernald, A., et al. (2006), Water quality changes in hyporheic flow paths between a large gravel bed river and off-channel alcoves in Oregon, USA, *RIVER RESEARCH AND APPLICATIONS*, *22*(10), 1111-1124.

Fischer, H. B., et al. (1979), *Mixing in Inland and Coastal Waters*, 302 pp., Elsevier Science & Technology Books.

Fowler, R., and R. Death (2001), The effect of environmental stability on hyporheic community structure, *HYDROBIOLOGIA*, *445*(1-3), 85-95.

Hannah, D., et al. (2004), Heat exchanges and temperatures within a salmon spawning stream in the cairngorms, Scotland: Seasonal and sub-seasonal dynamics, *RIVER RESEARCH AND APPLICATIONS*, 635-652.

Harvey, J., et al. (1996), Evaluating the reliability of the stream tracer approach to characterize stream-subsurface water exchange, *WATER RESOURCES RESEARCH*, *32*(8), 2441-2451.

Hulse, D., et al. (Eds.) (2002), *Willamette River Basin Planning Atlas*, Oregon State University Press, Corvallis.

Hyder, Z., and J. J. Butler (1995), Slug tests in unconfined formations: An assessment of the Bouwer and Rice technique, *Ground Water*, *33*(1), 6.

Johnson, A., et al. (2005), Evaluation of an inexpensive small-diameter temperature logger for documenting ground water-river interactions, *GROUND WATER MONITORING AND REMEDIATION*, *25*(4), 68-74.

Johnson, S. (2004), Factors influencing stream temperatures in small streams: substrate effects and a shading experiment, *CANADIAN JOURNAL OF FISHERIES AND AQUATIC SCIENCES*, 913-923.

Kasahara, T., and S. Wondzell (2003), Geomorphic controls on hyporheic exchange flow in mountain streams, *WATER RESOURCES RESEARCH*, -.

Kinouchi, T. (2007), Impact of long-term water and energy consumption in Tokyo on wastewater effluent: implications for the thermal degradation of urban streams, *HYDROLOGICAL PROCESSES*, *21*(9), 1207-1216.

Kinouchi, T., et al. (2007), Increase in stream temperature related to anthropogenic heat input from urban wastewater, *JOURNAL OF HYDROLOGY*, *335*(1-2), 78-88.

Landers, D., et al. (2002), Off Channel Habitats, in *Willamette Basin River Basin Planning Atlas: Trajectories of Environmental and Ecological Change*, edited by S. G. Dave Hulse, J. Baker, Oregon State University Press, Corvallis.

Leopold, L., et al. (1964), *Fluvial Processes in Geomorphology*, Dover, New York.

Loheide, S., and S. Gorelick (2006), Quantifying stream-aquifer interactions through the analysis of remotely sensed thermographic profiles and in situ temperature histories, *ENVIRONMENTAL SCIENCE & TECHNOLOGY*, 3336-3341.

Malard, F., et al. (2001), Thermal heterogeneity in the hyporheic zone of a glacial floodplain, *CANADIAN JOURNAL OF FISHERIES AND AQUATIC SCIENCES*, 1319-1335.

Neuman, S. P. (1990), Universal Scaling of Hydraulic Conductivites and Dispersivities in Geologic Media, *Water Resources Research*, *26*(8), 10.

O'Connor, J. E., et al. (2001), Origin, Extent, and Thickness of Quaternary Geologic Units in the Willamette Valley, Oregon, edited by U. S. G. Survey, USGS, Denver.

ODEQ (2006), Willamette Basin TMDL, edited by O. D. o. E. Quality.

Peterson, E., and T. Sickbert (2006), Stream water bypass through a meander neck, laterally extending the hyporheic zone, *HYDROGEOLOGY JOURNAL*, *14*(8), 1443-1451.

Poff, N., et al. (1997), The natural flow regime, *BIOSCIENCE*, *47*(11), 769-784.

Poole, G., and C. Berman (2001), An ecological perspective on in-stream temperature: Natural heat dynamics and mechanisms of human-caused thermal degradation, *ENVIRONMENTAL MANAGEMENT*, 787-802.

Reclamation, B. o. (2007), Agrimet, The Pacific Northwest Cooperative Agricultural Weather Network, edited, Bureau of Reclamation.

Selker, J., et al. (2006a), Distributed fiber-optic temperature sensing for hydrologic systems, *WATER RESOURCES RESEARCH*, *42*(12), -.

Selker, J., et al. (2006b), Fiber optics opens window on stream dynamics, *Geophysical Research Letters*, *33*(L24401), 4.

Silliman, S. E., and D. F. Booth (1993), Analysis of time-series measurements of sediment temperature for identification of gaining vs. losing portions of Juday Creek, Indiana., *Journal of Hydrology*, *146*, 17.

Sinokrot, B., and H. Stefan (1993), Stream Temperature Dynamics: Measurements and Modeling, *Water Resources Research*, *29*(7), 13.

Sinokrot, B., and H. Stefan (1994), Stream Water-Temperature Sensitivity to Weather and Bed Parameters, *Journal of Hydraulic Engineering*, *120*(6), 14.

Smart, P. L., and I. M. S. Laidlaw (1977), An evaluation of some fluorescent dyes for water tracing, *Water Resources Research*, *13*(1), 17.

Soerens, T. S., and D. A. Sabatini (1994), Cosolvency Effects on Sorption of a Semipolar, Iongenic Compound (Rhodamine WT) with Subsurface Materials, *Environmental Science and Technology*, *28*, 5.

Stallman, R. W. (1965), Steady One-Dimensional Fluid Flow in a Semi-Infinite Porous Medium with Sinusoidal Surface Temperature, *Journal of Geophysical Research*, *70*(12), 7.

Story, A., et al. (2003), Stream temperatures in two shaded reaches below cutblocks and logging roads: downstream cooling linked to subsurface hydrology, *CANADIAN JOURNAL OF FOREST RESEARCH-REVUE CANADIENNE DE RECHERCHE FORESTIERE*, *33*(8), 1383-1396.

Taniguchi, M. (1993), Evaluation of Vertical Groundwater Fluxes and Thermal Properties of Aquifers Based on Transient Temperature-Depth Profiles, *Water Resources Research*, *29*(7), 6.

Todd, and Davis (2005), *Groundwater Hydrology*, Third ed., John Wiley & Sons, Inc.

Torgersen, C., et al. (1999), Multiscale thermal refugia and stream habitat associations of chinook salmon in northeastern Oregon, *ECOLOGICAL APPLICATIONS*, *9*(1), 301-319.

Webb, B., and Y. Zhang (2004), Intra-annual variability in the non-advective heat energy budget of Devon streams and rivers, *HYDROLOGICAL PROCESSES*, 2117-2146.

White, D. S. (1993), Perspectives on defining and delineating hyporheic zones, *Journal of North American Benthological Society*, *12*(1), 9.

APPENDICIES

6. APPENDIX A: METHODS

6.1 Piezometer Installation

A steel well driver, “potato masher” was used to install 3.175 cm diameter PVC pipe around the alcoves. The well driver consists of a hollow, outer shell (slightly larger than the PVC pipe) and a solid, inner, steel driving rod with a steel head. The steel head has a larger diameter than the outer shell and is the contact/driving point between the outer shell and the driving rod. The procedure to install a PVC pipe is outlined as follows: the outer shell is driven into the ground by either lifting the driving rod and allowing the steel head to force the outer shell into the substrate, or by striking the head of the inner rod with a sledge hammer. Once the entire device is driven to the desired depth, the inner rod is removed and a PVC pipe is lowered in its place. The outer shell is then pulled out of the substrate leaving the PVC pipe securely in the ground.

6.2 Measuring Water Level and Gradient

Water levels within each piezometer were measured with a metal tape measure and wet erase marker. A line is drawn on the tape measure with the wet erase marker that is the same length as the piezometer. The tape measure is then inserted into the piezometer until the end touches the bottom. The water in the piezometer will dissolve the line on the measuring tape below the water level. The distance from the top of the piezometer to the water line subtracted from the total piezometer length equals the elevation of the water in the piezometer.

The change in water level height is found by subtracting the water level in the alcove with the water level in the alcove. The change in distance is the length from the

piezometer to the water surface of the alcove. Dividing the change in height by the change in distance equals the gradient.

6.3 Hydraulic Conductivity

The hydraulic conductivity of the alluvium around the alcove was calculated using the Bouwer-Rice method (*Bouwer and Rice*, 1976; *Bouwer*, 1989; *Hyder and Butler*, 1995).

First, slug tests were performed to measure the response time of water levels inthe piezometer using 1 L slugs of water. Slug tests were repeated 3 times at every piezometer, each time allowing the water level to re-equilibrate with ambient head before performing the next test. Slug tests at Pope and Talbot were only performed once due to the low hydraulic conductivity of the alluvium around many of the piezometers.

$$K = \frac{r_c^{\,2} \ln(R_e / r_w)}{2L_e} \frac{1}{T_o} \tag{7}$$

$$\ln \frac{R_e}{r_w} = \left[\frac{1.1}{\ln(L_w / r_w)} + \frac{A + B \ln[H - L_w) / r_w]}{L_e / r_w} \right]^{-1} \tag{8}$$

See (*Todd and Davis*, 2005) for parameter definitions. After slug tests are performed, equation 7 can be populated using measurements from the piezometer and equation 8. "*H*," in equation 8, is the distance between the static water level and the base of the aquifer, and was assumed to be 20 m. Due to the large hydraulic conductivity of the alluvium in some places of the alcoves, the piezometer itself was limiting the drawdown time.

6.4 Tracer Test

Tracer tests were performed in each alcove to measure the flux of water moving out of the alcove and into the mainstem of the river. To find the flux of water moving into the mainstem (m^3/s) the concentration of the tracer (Rhodamine WT) is measured using a fluorometer. The measurements begin before the tracer is released (to record background levels) and continue until all of the tracer has passed and concentrations have returned to background levels. Plotting the tracer concentrations against time produces a break through curve (Figure 13). The area under the break through curve is equal to the 0^{th} moment which is found by numerically integrating the curve using the trapezoidal rule. The flux of the alcove can then be calculated using the equation:

$$Q_{Total} = \frac{M}{m_o} \tag{9}$$

Q_{Total} = Alcove flow rate, m^3/s; M = Mass of tracer, g; m_o = 0^{th} moment (area under breakthrough curve),g/m^3s.

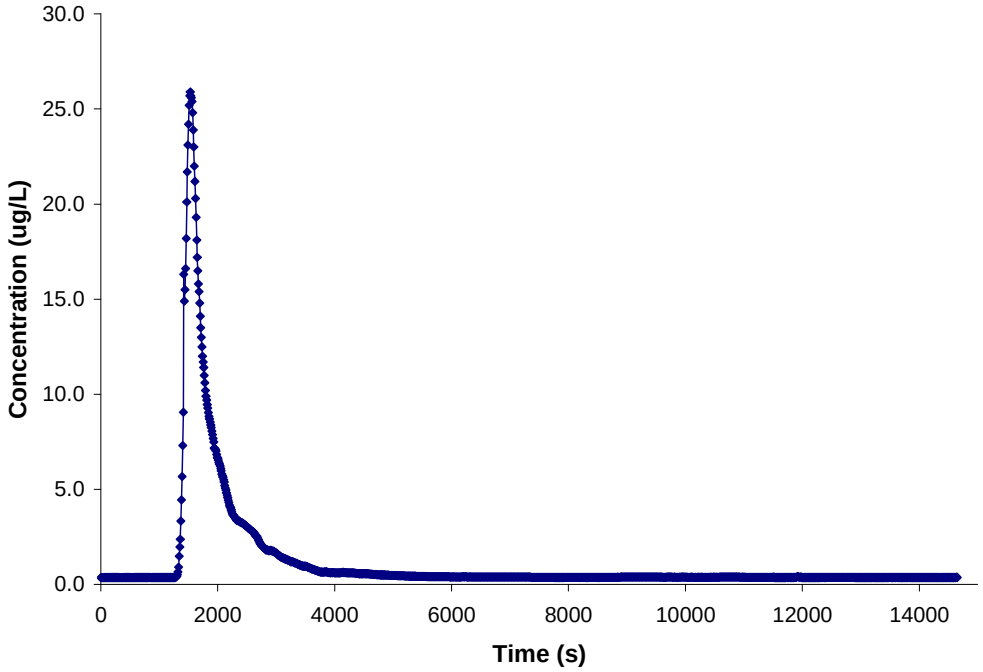

Figure 12. Breakthrough curve for tracer test at Harrisburg Bar, 8/07/07, 11:00 am.

6.5 Dispersion Calculations

Two dispersion calculations were performed for this study. The first was for dispersion of the alcove surface water and was used in the W2 model (*Fischer et al.*, 1979).

$$D_{sufrace} = 5.93 \times d \times u^{*} \quad (10)$$

$D_{surface}$ = Dispersion coefficient at water surface, m^2/s; d = average depth of alcove, m; u^{*} = shear velocity, m/s.

$$u^{*} = \sqrt{g \times h \times S_o} \quad (11)$$

g = gravity, m/s^2; h = flow depth, m; S_o = slope, -.

The second dispersion value was used in the Stallman equation and is used for dispersion in the subsurface for hyporheic water moving through the gravel bar and into the alcove. α is the longitudinal dispersivity, m (*Neuman*, 1990).

$$D_{horizontal} = D_{longitudinal} + (k / c\rho) \quad (12)$$

$$D_{longitudinal} = v \times \alpha \quad (13)$$

$$\alpha = 0.017 \times L^{1.5} \quad (14)$$

v = velocity (varied), cm/s; L = length, m; k=0.0059, J/(s cm ^{o}C); c = 1.67, J/g^{o}C; ρ=1.954 g/cm^3.

$$T - T_A = \Delta T\left(e^{-az}\right) \times \sin(2\pi t / \tau - bx) \quad (15)$$

T = temperature at any point x, t, ^{o}C; T_A = average ambient temperature x, t at the land surface, ^{o}C; ΔT = amplitude of the temperature variation at the surface, ^{o}C;

$a=((U^2+V^4/4)^{1/2}+V^2/2)^{1/2}-V$; $b=((U^2+V^4/4)^{1/2}-V^2/2)^{1/2}$; $U=\frac{\pi}{\tau}\left(\frac{k}{c\rho}+D_L\right)^{-1}$;

$V=\frac{vc_o\rho_o}{2c\rho}\left(\frac{k}{c\rho}+D_L\right)^{-1}$; c = specific heat of the fluid and rock in combination, cal/(g^{o}C); c_r = specific heat of the rock, cal/(g^{o}C); c_o = specific heat of the fluid, cal/(g^{o}C); k = heat conductivity of fluid and solid in combination, cal/(s*cm^{o}C); t = time, sec; v = velocity of water along the flow path, cm/s; x = distance along flow path, cm; ρ = density of fluid and rock in combination, g/cm^3; ρ_o = density of fluid, g/cm^3; ρ_r = density of rock, g/cm^3; τ = period of oscillation of temperature at land surface, s.

7. APPENDIX B: FIELD DATA RESULTS

7.1 Field Data

Graphs showing water temperature data from thermistors in piezometers and alcoves.

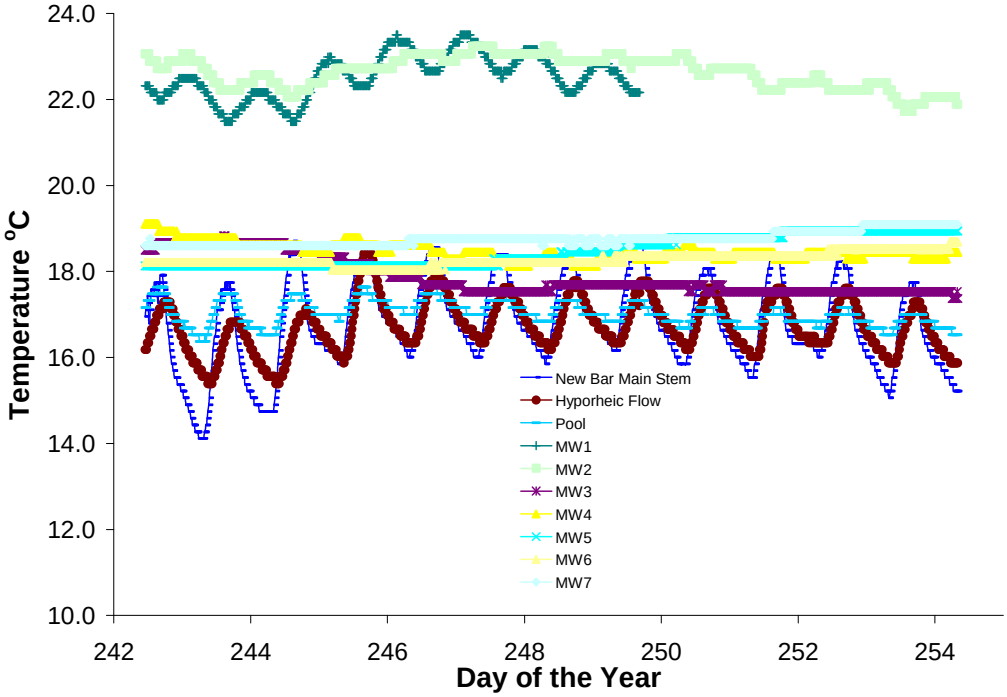

Figure 13. Water temperature at Harrisburg Bar, 8/30/06 to 9/11/06.

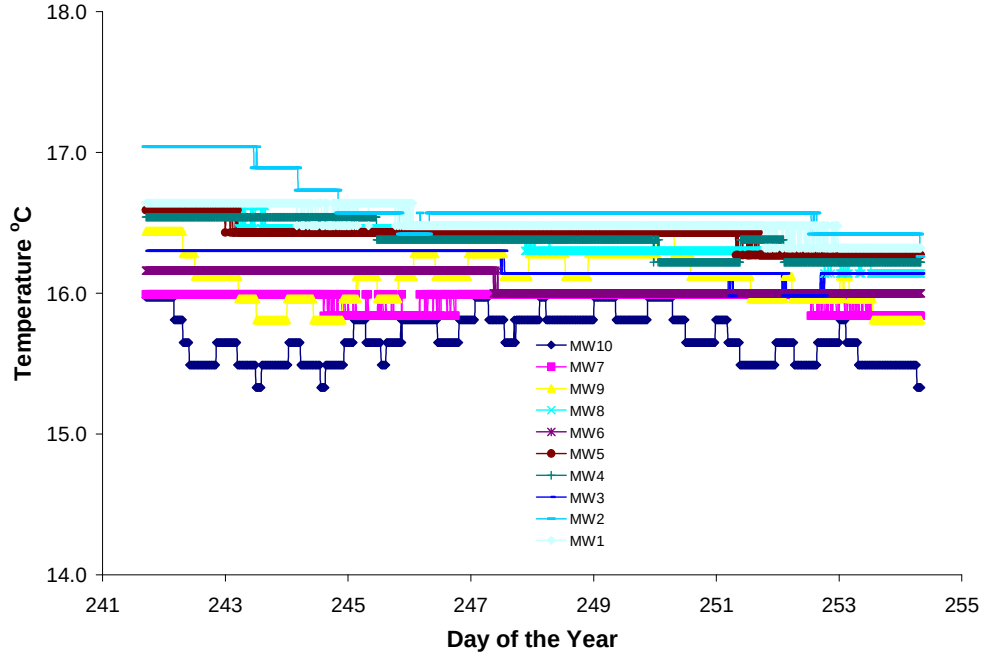

Figure 14. Green Island piezometer temperatures, 8/29/06 – 9/08/06.

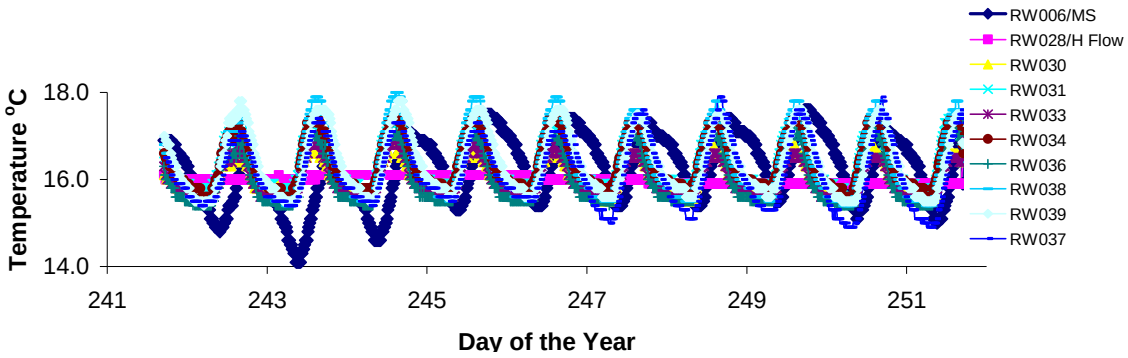

Figure 15. Green Island alcove temperatures, 8/29/06 – 9/08/06.

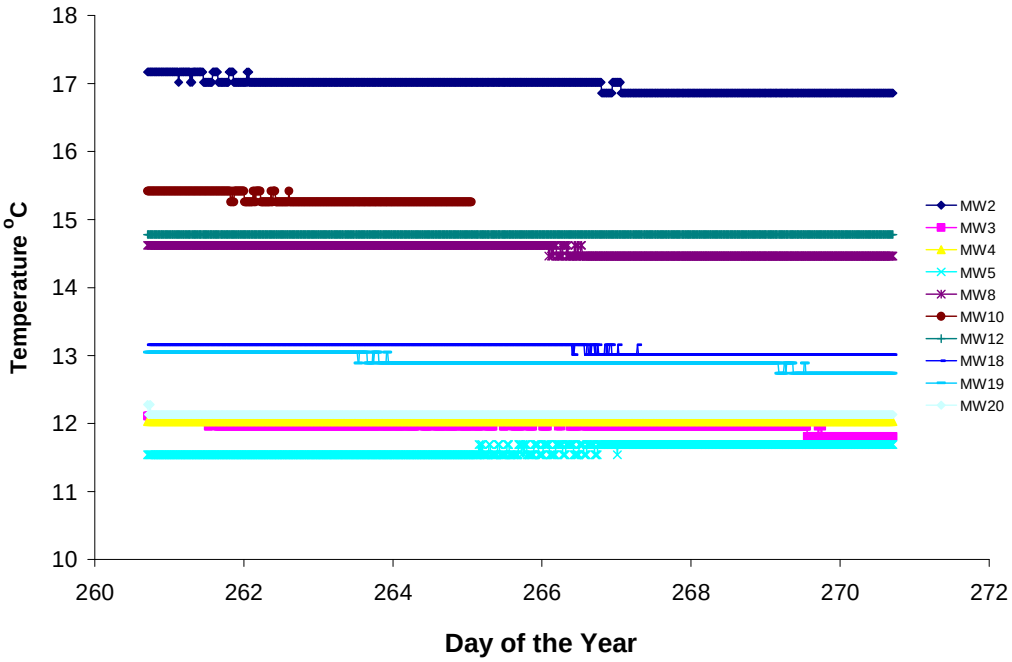

Figure 16. Norwood Slough, piezometer water temperatures, 9/17/06 – 9/27/06.

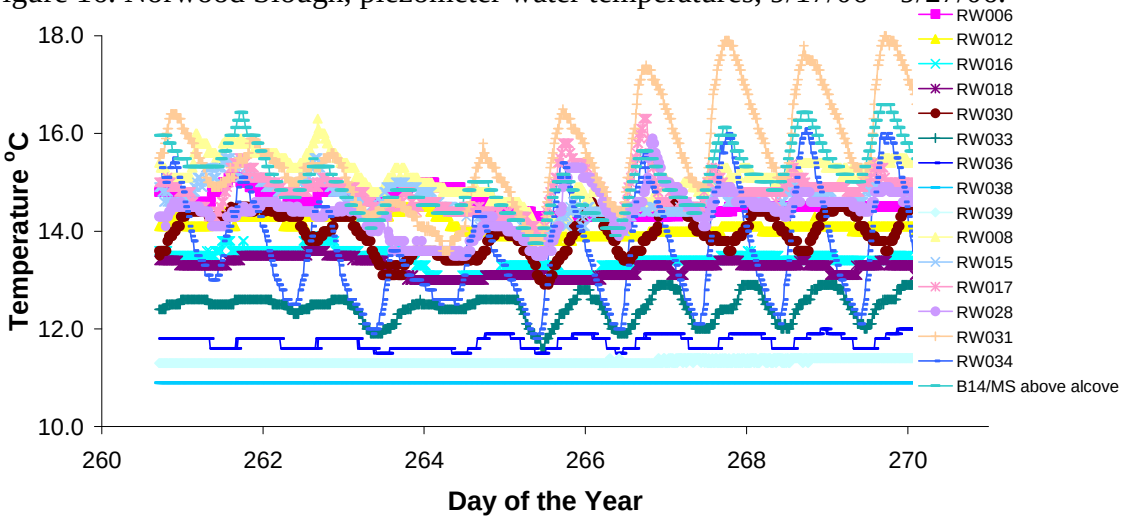

Figure 17. Norwood Slough, alcove water temperatures, 9/17/06 – 9/27/06.

7.2 Air Temperature

Graphs showing air temperature data from recorders placed around the alcoves.

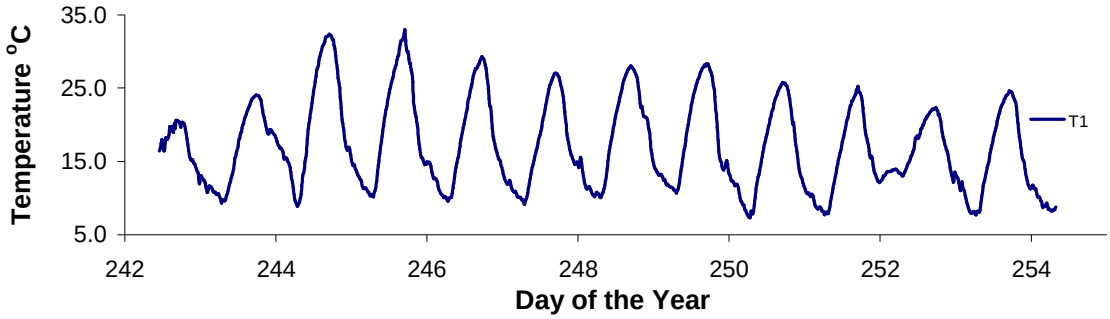

Figure 18. Harrisburg Bar air temperature, 8/30/06 – 9/11/06.

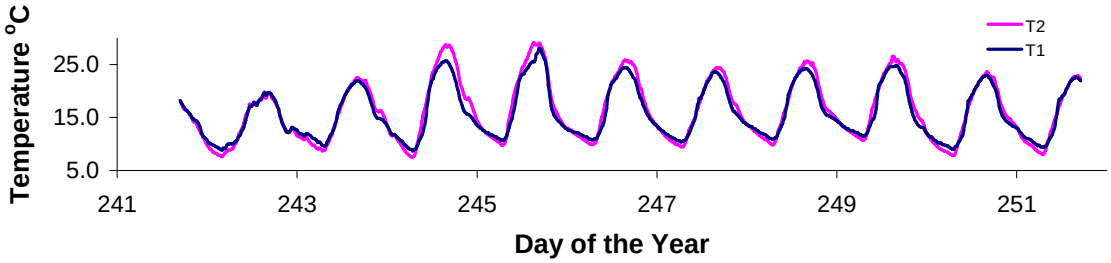

Figure 19. Green Island air temperature, 8/29/06 – 9/08/06.

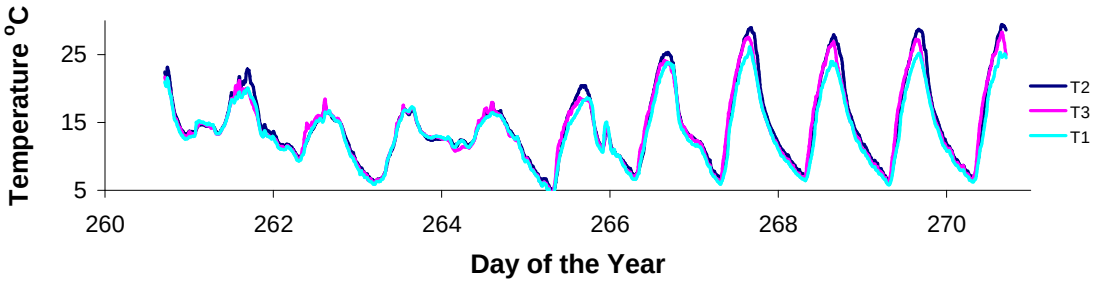

Figure 20. Norwood Slough air temperature, 9/17/06 – 9/27/06.

7.3 Meteorological Data

Data that could not be recorded in the field were downloaded from the Agrimet Weather Station between Corvallis and Albany on Highway 20 (Latitude 44° 38’ 03”,

Longitude 123° 11’ 24”, elevation: 230’; installed on 2/27/90). Data obtained from Agrimet station included dew point temperature, solar radiation, wind speed and wind direction. Weather data can be accessed via the website: http://www.usbr.gov/pn/agrimet/agrimetmap/crvoda.html (last accessed 11/03/07).

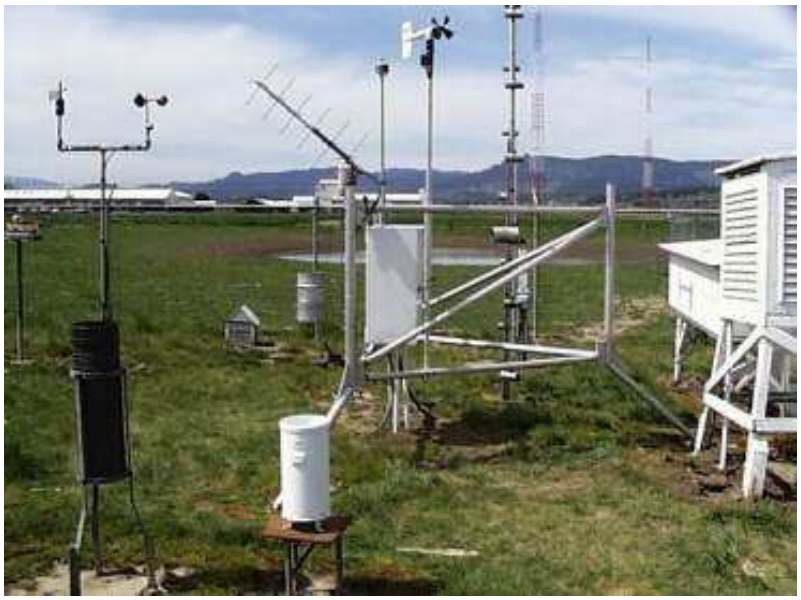

Figure 21. Corvallis Agrimet Station.

Table 5. Agrimet equipment and sensors.

Equipment	Manufacturer	
Data Logger Model CR10X	Campbell Scientific, Inc.	
GOES Transmitter Model TGT-1	Telonics, Inc.	
Yagi Antenna, Model 5000-0080	Sutron, Inc.	
10 Watt Solar Panel Model MSX-10	Solarex, Inc.	
31-PHD Workaholic Battery	Interstate Batteries, Inc.	
Station Tripod	U.S. Bureau of Reclamation	
NEMA 4-E Enclosure Model A-24 H20 CLP	Hoffman, Inc.	
Sensors	**Manufacturer**	**Sensor Height**
Pyranometer Model LI-200SB	Licor, Inc.	3 meters
Wind Monitor Model 05103	RM Young, Inc.	2 meters
Air Temperature Thermistor Model 44030	YSI, Inc.	2 meters
Relative Humidity Sensor Model HMP 35A/45D	Vaisala, Inc.	2 meters
Temperature/RH Radiation Shield Model 41002P	RM Young, Inc.	2 meters
Tipping Bucket Precipitation Gage Model 6011A/6010	Qualimetrics, Inc.	2 meters
Universal Storage Precipitation Gage	Belfort, Inc.	2 meters

7.4 Tracer Test Results

Tracer tests were performed in each alcove to measure the flux of water moving into the mainstem. Results were used as Q_{total} in the W2 model. Tracer tests at Norwood Slough were repeated multiple times due to equipment failure and beavers destroying equipment.

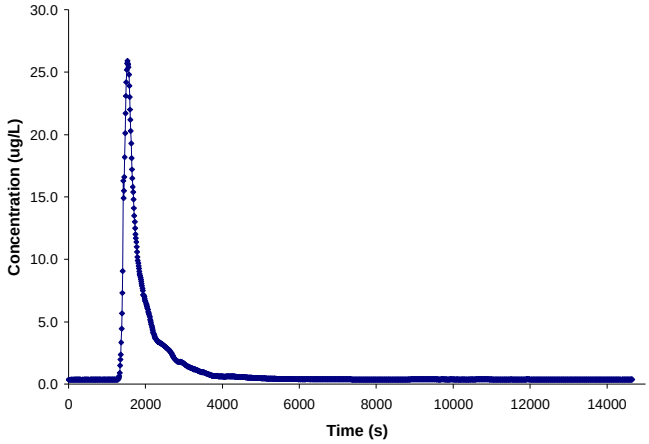

Figure 22. Tracer test at Harrisburg Bar on 8/07/06, 11:00 am.

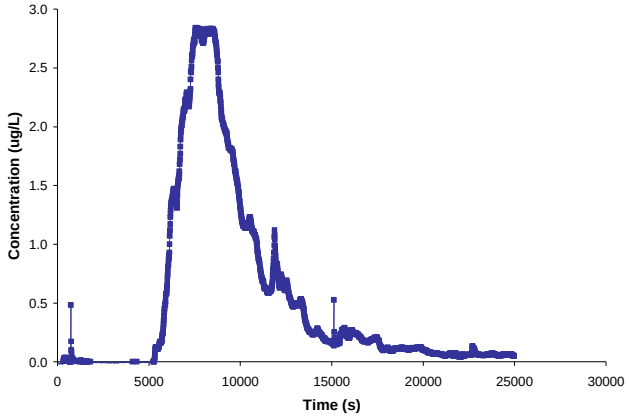

Figure 23. Tracer test at Green Island on 8/24/06, 10:22 am.

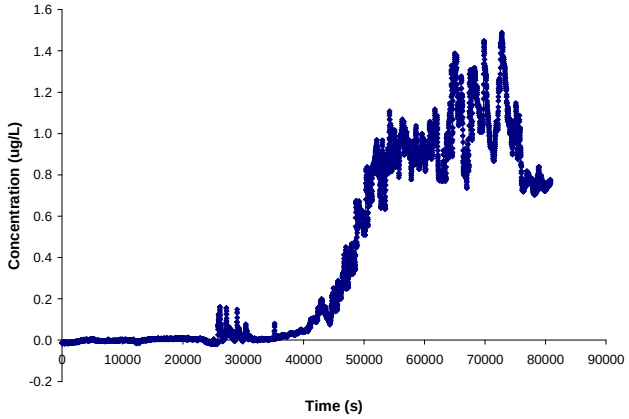

Figure 24 Tracer Test at Norwood Slough on 10/02/06, 2:23 pm.

7.5 Slug Test Results

Sample drawdown curves are shown for each site. The remaining curves are presented in Appendix_E.

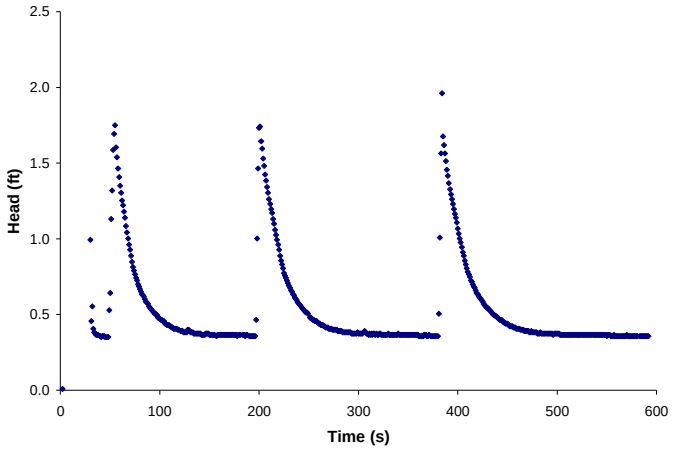

Figure 25. Drawdown curve for MW8 on Harrisburg Bar, 8/16/07.

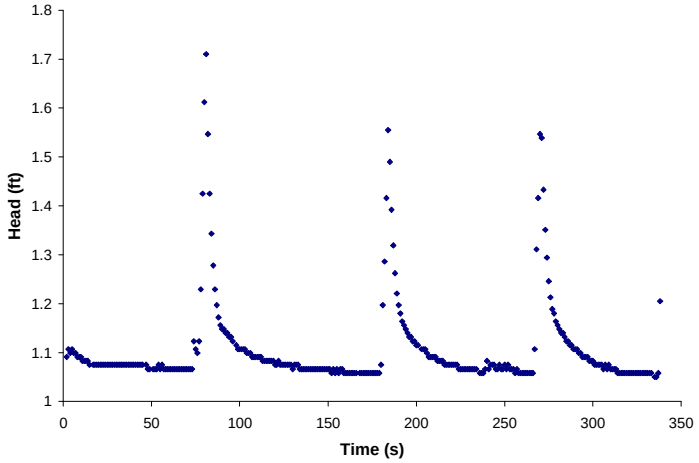

Figure 26. Drawdown curve for MW10 on Green Island, 8/24/07.

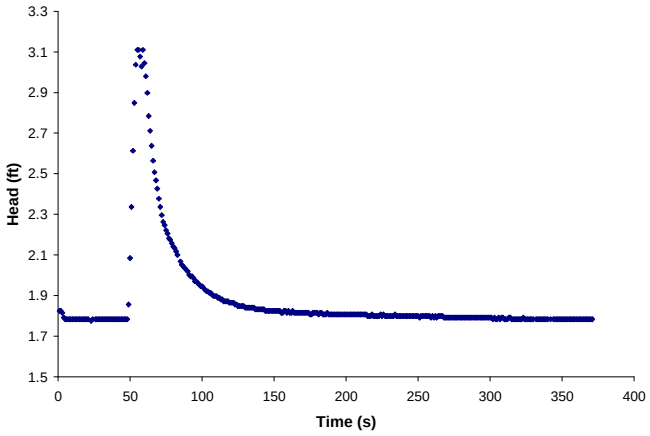

Figure 27. Drawdown curve for MW10 on Norwood Slough. 8/17/07.

7.6 Calculated Hydraulic Conductivities

Table 6. Harrisburg Bar hydraulic conductivities (*K*).

Well ID	K avg (m/s)	Method
MW1	1.85×10^{-4}	Bouwer-Rice
MW2	5.28×10^{-4}	Bouwer-Rice
MW3	5.95×10^{-4}	Bouwer-Rice
MW4	1.75×10^{-3}	Bouwer-Rice
MW5	Not Calculated	
MW6	Not Calculated	
MW7	Not Calculated	
MW8	4.80×10^{-5}	Bouwer-Rice
MW9	1.57×10^{-4}	Bouwer-Rice
MW10	1.79×10^{-4}	Bouwer-Rice
MW11	4.83×10^{-5}	Bouwer-Rice

Table 7. Green Island hydraulic conductivities (*K*).

Well ID	K avg (m/s)	Method
MW1	4.26×10^{-4}	Bouwer-Rice
MW2	1.72×10^{-4}	Bouwer-Rice
MW3	Not Calculated	
MW4	Not Calculated	
MW5	Not Calculated	
MW6	Not Calculated	
MW7	4.33×10^{-4}	Bouwer-Rice
MW8	Not Calculated	
MW9	8.04×10^{-5}	Bouwer-Rice
MW10	1.94×10^{-4}	Bouwer-Rice

Table 8. Norwood Slough hydraulic conductivities (*K*).

Well ID	K (m/s)	Method
MW2	8.68×10^{-6}	Bouwer-Rice
MW4	4.72×10^{-5}	Bouwer-Rice
MW5	6.37×10^{-5}	Bouwer-Rice
MW8	3.32×10^{-5}	Bouwer-Rice
MW10	7.88×10^{-5}	Bouwer-Rice
MW12	5.04×10^{-6}	Bouwer-Rice
MW18	Not Calculated	
MW19	Not Calculated	
MW20	Not Calculated	

7.7 GPS Figures

Alcove outlines and features were recorded by walking along the perimeter of each site using a GPS, WGS 1984 datum (Pathfinder PRO XRS, Trimble, Sunnyvale, CA, USA.) Dark areas represent unvegetated gravel bars.

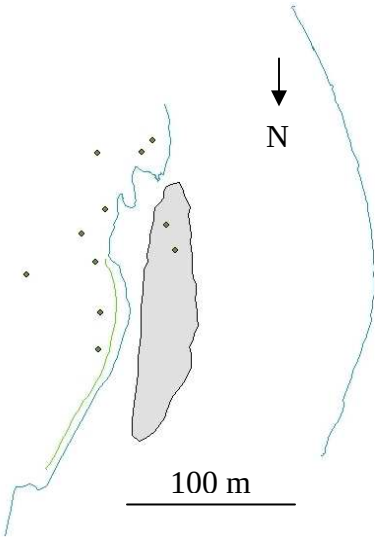

Figure 28. Outline of Harrisburg Bar with piezometer locations, 8/16/06.

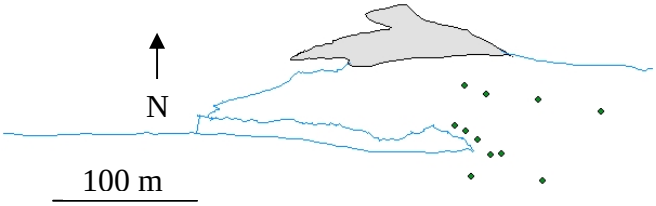

Figure 29. Outline of Green Island with piezometer locations 9/06/06.

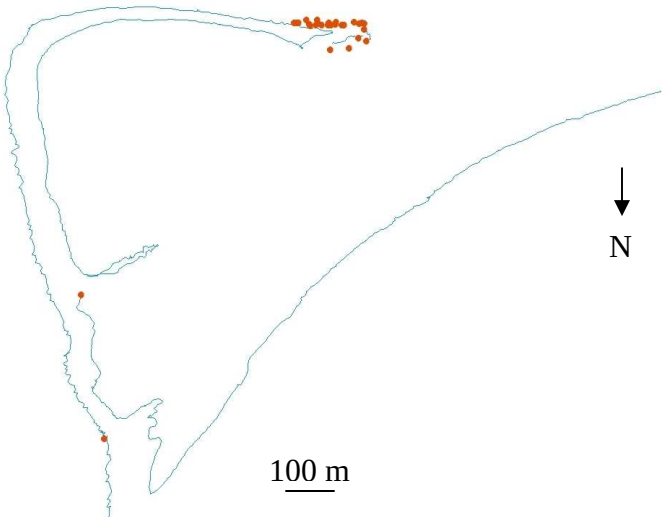

Figure 30. Outline of Norwood Slough; piezometer locations and alcove features, 8/18/06.

7.7 Cross sectional profiles

Cross sectional profiles were measured using a measuring tape and stadia rod. Depth measurements were recorded are regular intervals across the alcove's channel. The first cross section of each alcove is presented below, the remaining profiles along with their coordinate locations can be found in Appendix_CD.

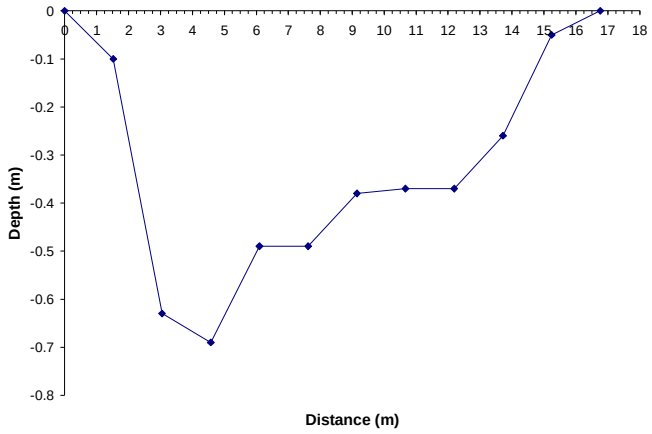

Figure 31. Cross section #1 of Harrisburg Bar, 44°15'09.55" N, 123°10'42.06" W.

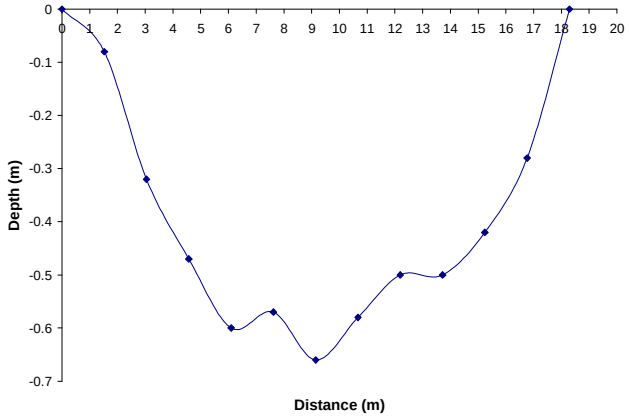

Figure 32. Cross section #1 of Green Island 44°08'39.15" N 123°07'27.41" W.

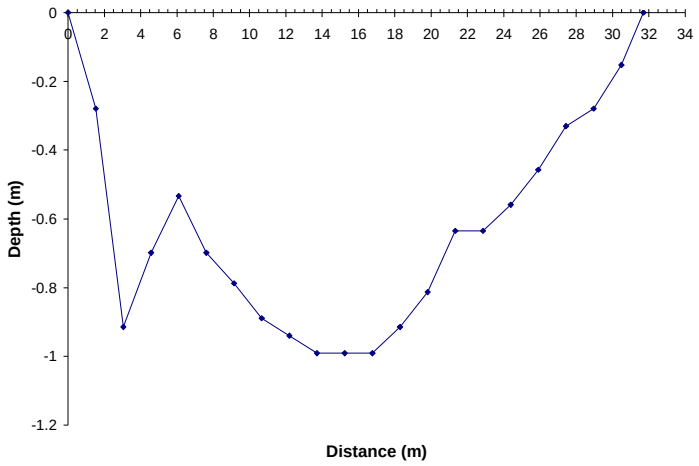

Figure 33. Cross section #1 of Norwood Slough, 44°23’02.76” N,123°13’36.39” W.

7.8 Hydraulic gradients

Hydraulic gradients were measured by dividing the change in water level elevation in the piezometer to the alcove's water surface by the distance from the piezometer to the alcove's water surface.

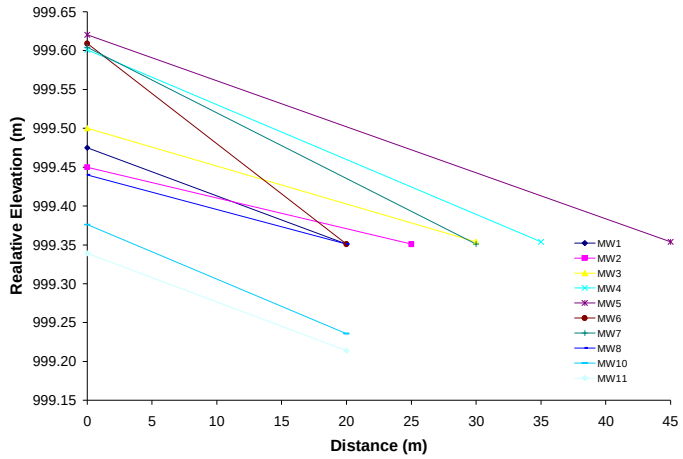

Figure 34. Hydraulic gradients at Harrisburg Bar on 9/14/06.

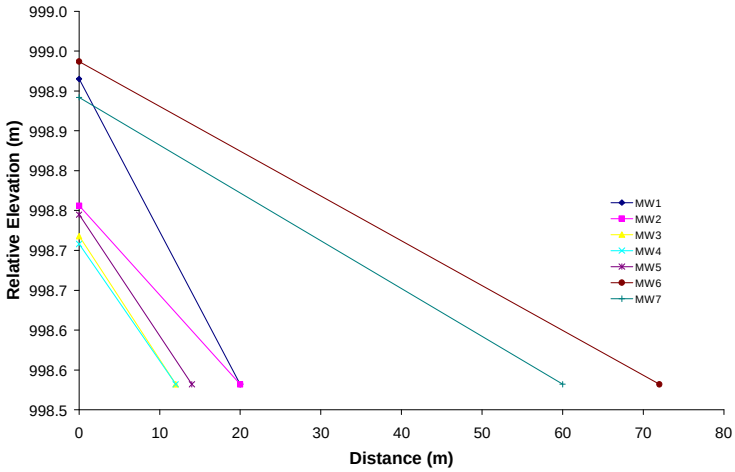

Figure 35. Hydraulic gradients at Green Island on 9/15/06.

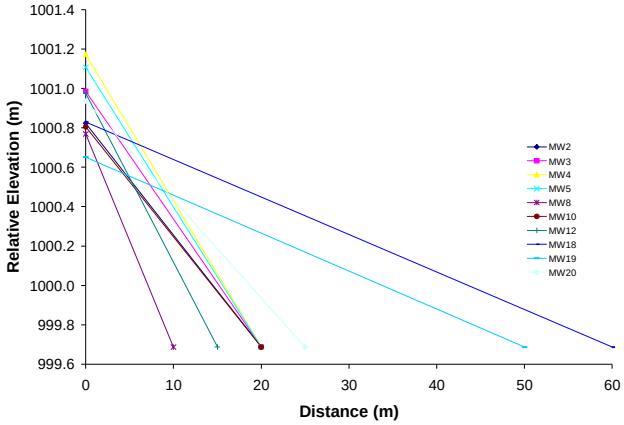

Figure 36. Hydraulic gradients at Norwood Slough on 9/14/06.

7.9 Inflow calculations

Inflow fluxes into the alcoves were calculated using the Dupuit Equation and calculated *K* values . The calculated fluxes below were used as a starting point for building each site model.

Table 9. Inflow calculations for Harrisburg Bar using the Dupuit equation.

	West Side/Low Grad (gravel bar)	East Side/High Grad	South End (head of bar)
q **(m^2/s) =**	4.80E-05	1.43E-04	1.65E-04
K **(m/s) =**	3.00E-04	0.0003	8.00E-04
x **(m) =**	20	20	30
h_o (m) **=**	10.315	10.913	10.6
h (m) **=**	10	10	10

	q (m2/s)	Length (m)	Q=q*length (m3/s)
gravel bar	4.80E-05	191	0.009
bank	1.43E-04	227	0.033
head of bar	1.65E-04	25	0.004

Table 10. Inflow calculations for Green Island using the Dupuit equation.

	Point Bar Side (RB) MW1	Bank Side (LB)	Hyporheic Flow (head of bar) MW5
q **(m^2/s) =**	7.62E-05	9.70E-05	5.31E-03
K **(m/s) =**	4.26E-04	4.30E-04	1.00E-02
x **(m) =**	18	15	5
h_o (m) **=**	15.213	15.224	15.176
h (m) **=**	15	15	15

	q (m2/s)	Length (m)	Q=q*length (m3/s)
Pt Bar Side	7.62E-05	200	0.015
Bank	9.70E-05	205	0.020
Head of Bar	$5.31x10^{-3}$	44	$2.34x10^{-1}$

Table 11. Inflow calculations for Norwood Slough using the Dupuit equation.

	River Side	Bank	Upwelling
q **(m^2/s)=**	1.79×10^{-4}	4.07×10^{-4}	2.06×10^{-4}
K **(m/s) =**	3.14×10^{-5}	5.54×10^{-5}	1.00×10^{-3}
x **(m) =**	20	20	30
h_o ***(m) =***	100.823	101.15	10.6
h (m) =	99.687	99.687	10

	q (m^2/s)	Length (m)	Q=q*length (m^3/s)
River Side	1.79×10^{-4}	1527	0.273
Bank	4.07×10^{-4}	1527	0.621
Upwelling	2.06×10^{-4}	25	5.00×10^{-3}

8. APPENDIX C: MODEL RESULTS

Models were calibrated to observed temperature by minimizing the RMSE between modeled alcove temperature and observed alcove temperature at head of the alcove (A23, RW030, and RW036 for Harrisburg Bar, Green Island, and Norwood Slough, respectively).

Harrisburg Bar

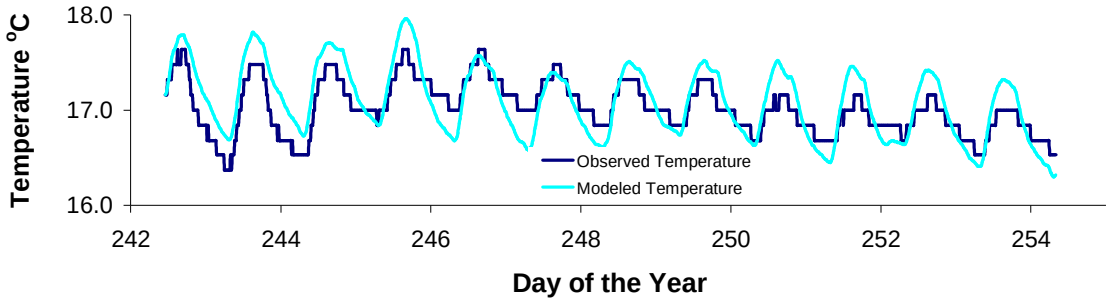

Figure 37. Segment 2, Harrisburg Bar, best calibrated model.

Green Island

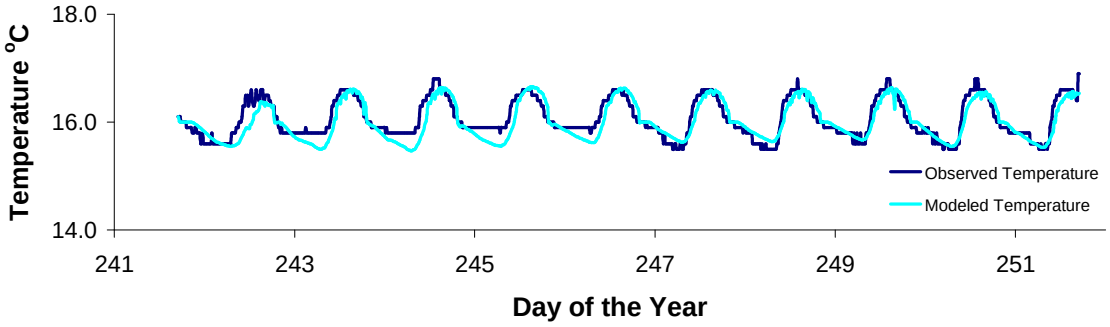

Figure 38. Segment 2, Green Island, best calibrated model.

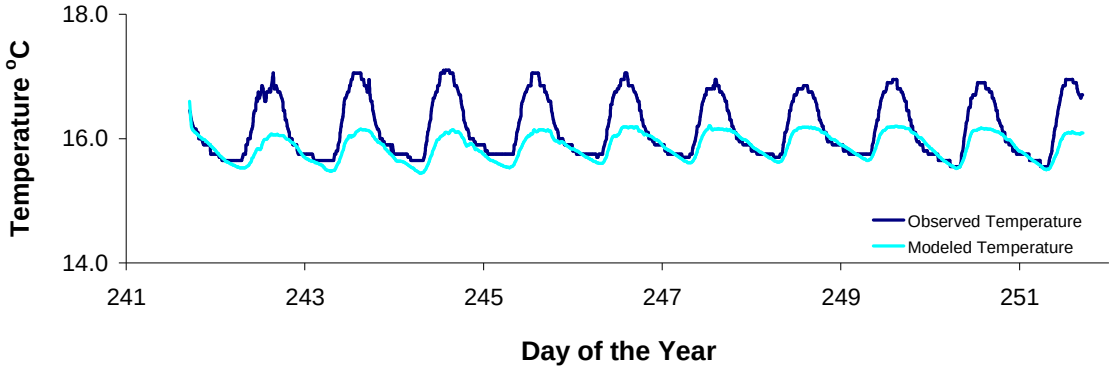

Figure 39. Segment 3, Green Island, best calibrated model.

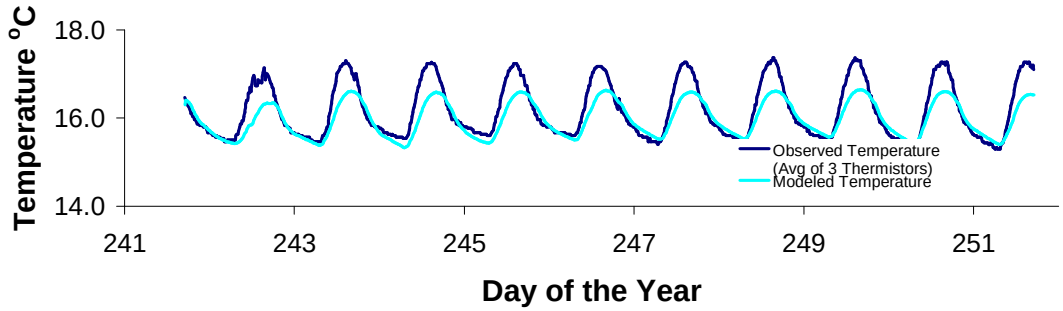

Figure 40. Segment 4, Green Island, best calibrated model.

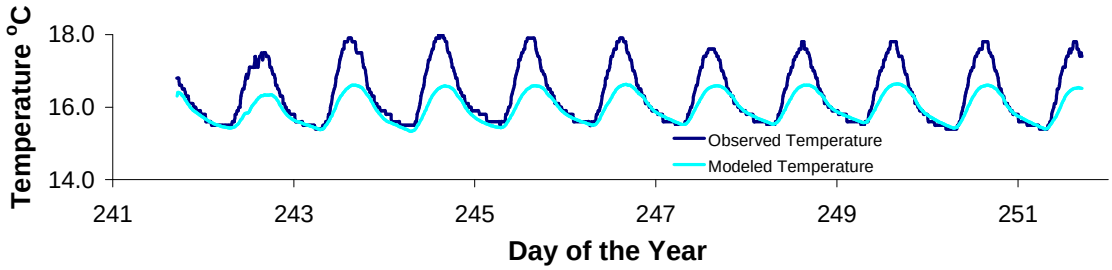

Figure 41. Segment 5, Green Island, best calibrated model.

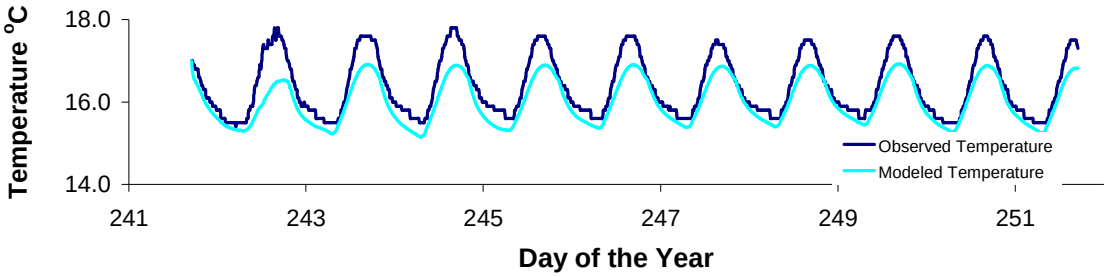

Figure 42. Segment 6, Green Island, best calibrated model.

Norwood Slough

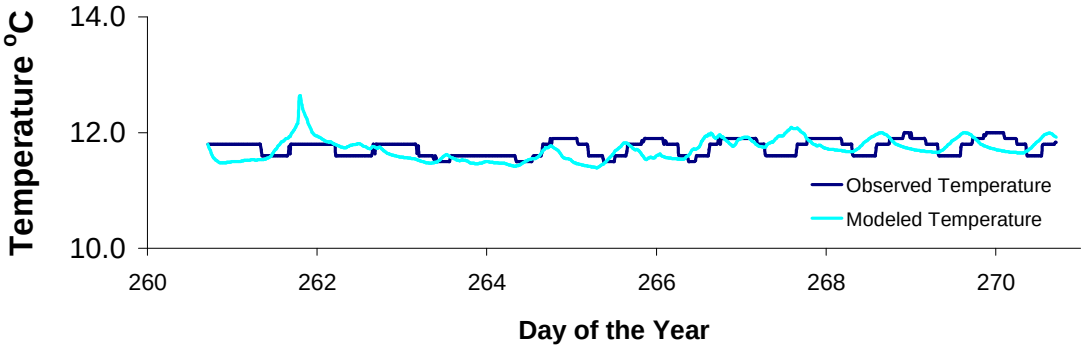

Figure 43. Segment 3, Norwood Slough, best calibrated model.

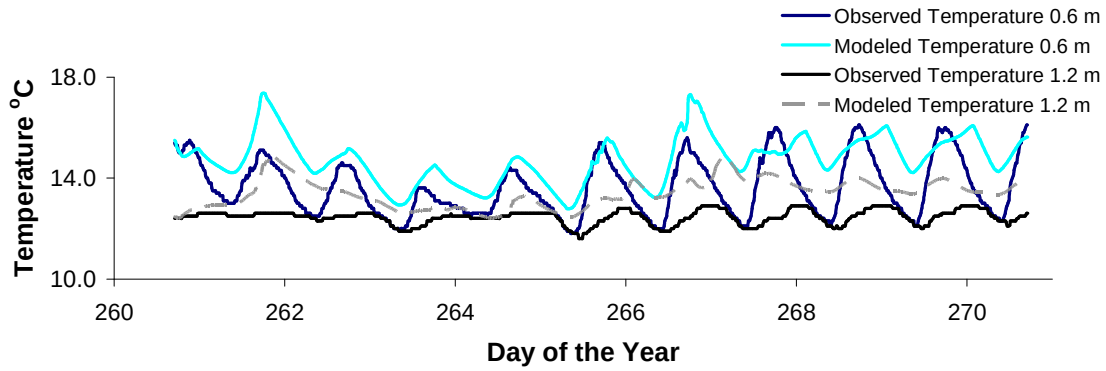

Figure 44. Segment 4, Norwood Slough, best calibrated model.

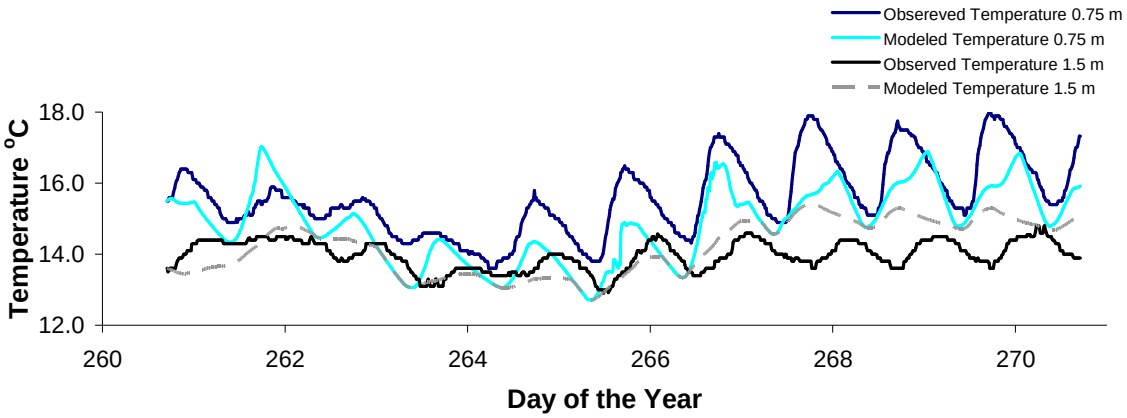

Figure 45. Segment 5, Norwood Slough, best calibrated model.

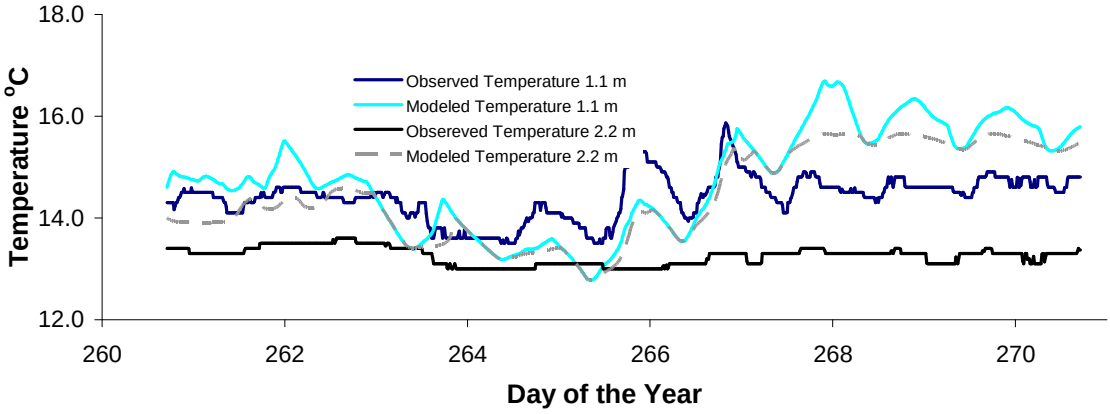

Figure 46. Segment 6, Norwood Slough, best calibrated model.

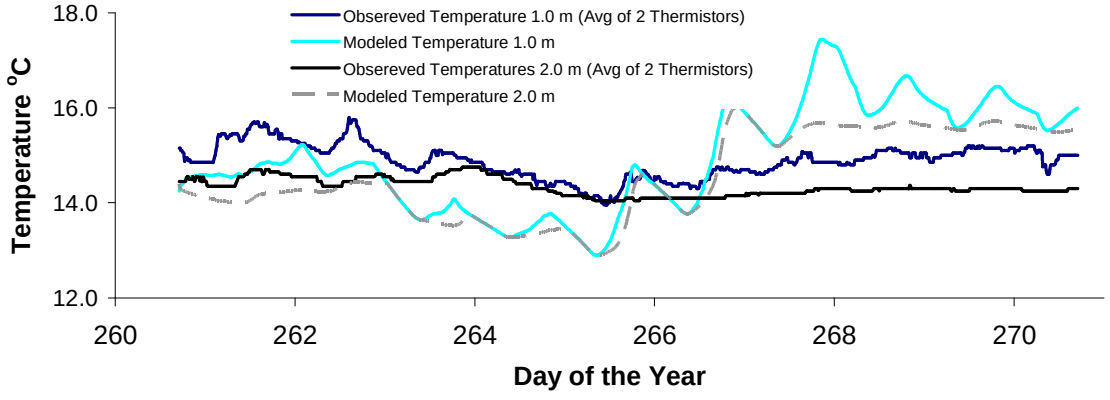

Figure 47. Segment 7, Norwood Slough, best calibrated model.

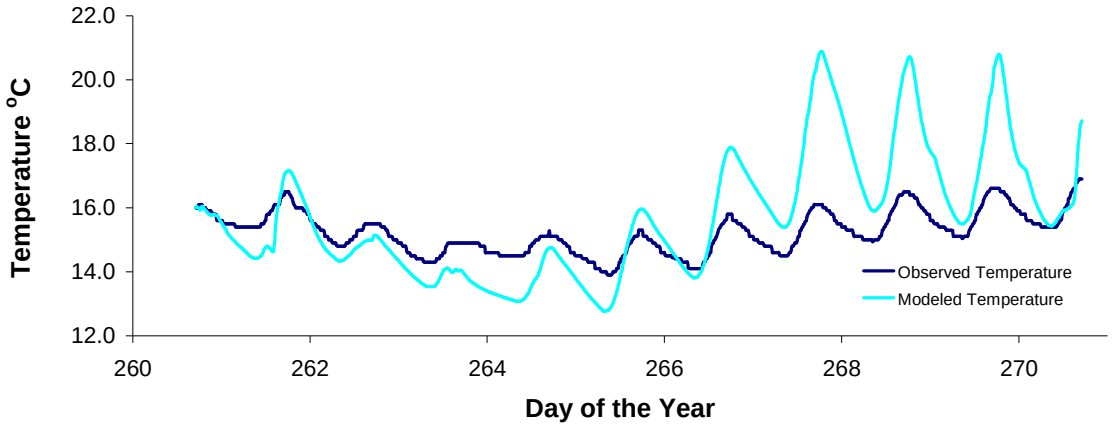

Figure 48. Segment 9, Norwood Slough, best calibrated model.

9.0 APPENDIX D: ANALYSIS RESULTS

9.1 Projected Alcove Temperature

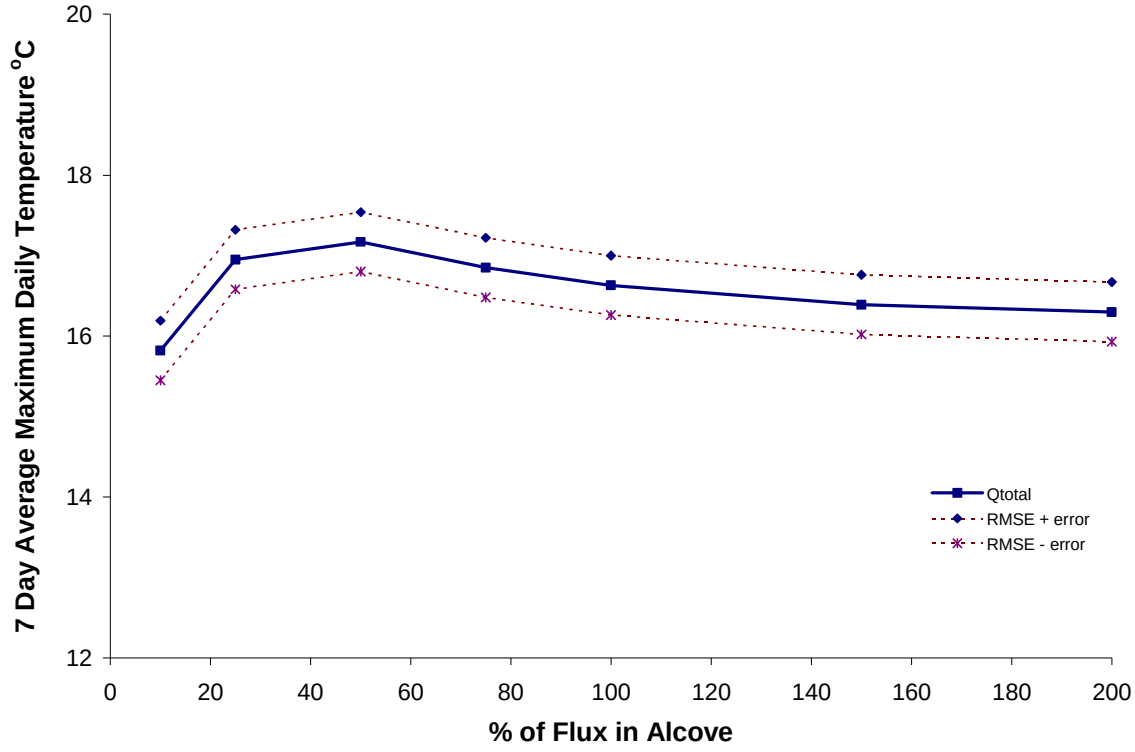

Figure 49. Green Island, effect of flux on alcove temperature.

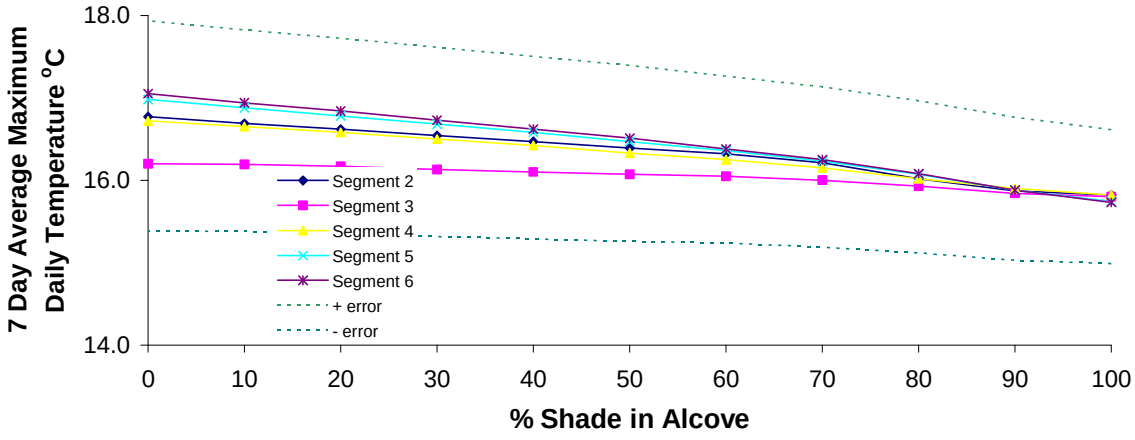

Figure 50. Green Island, effect of shade on alcove temperature.

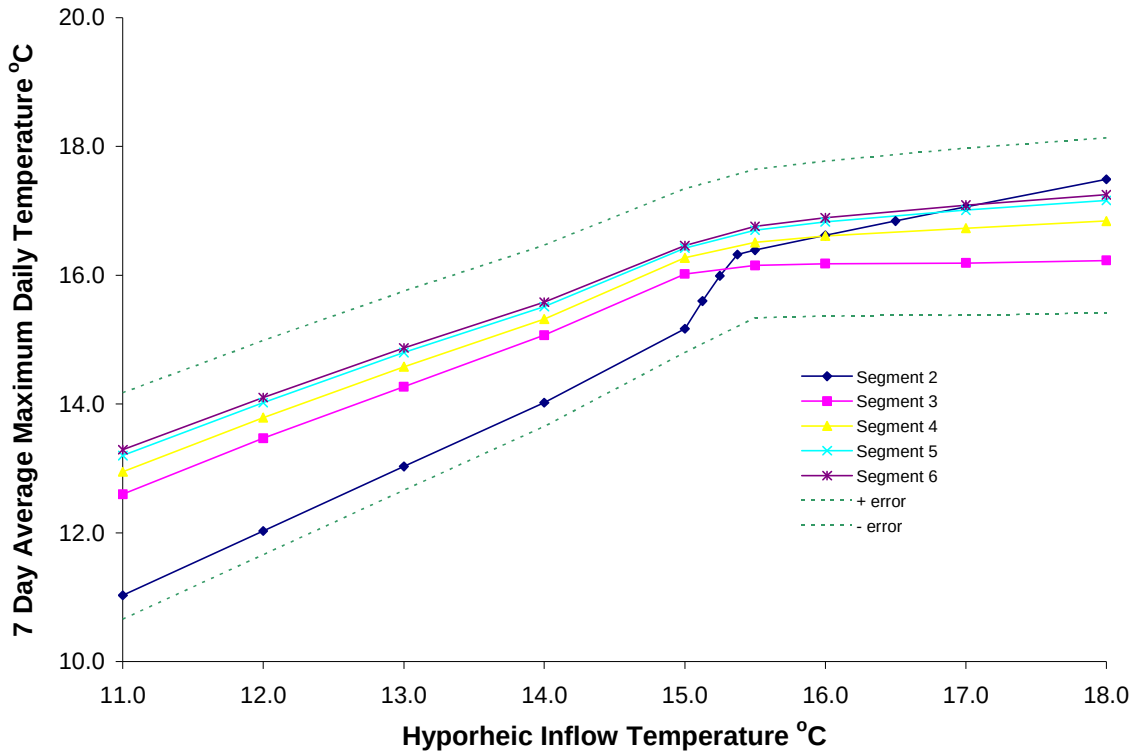

Figure 51. Green Island, effect of hyporheic inflow temperature on alcove temperature.

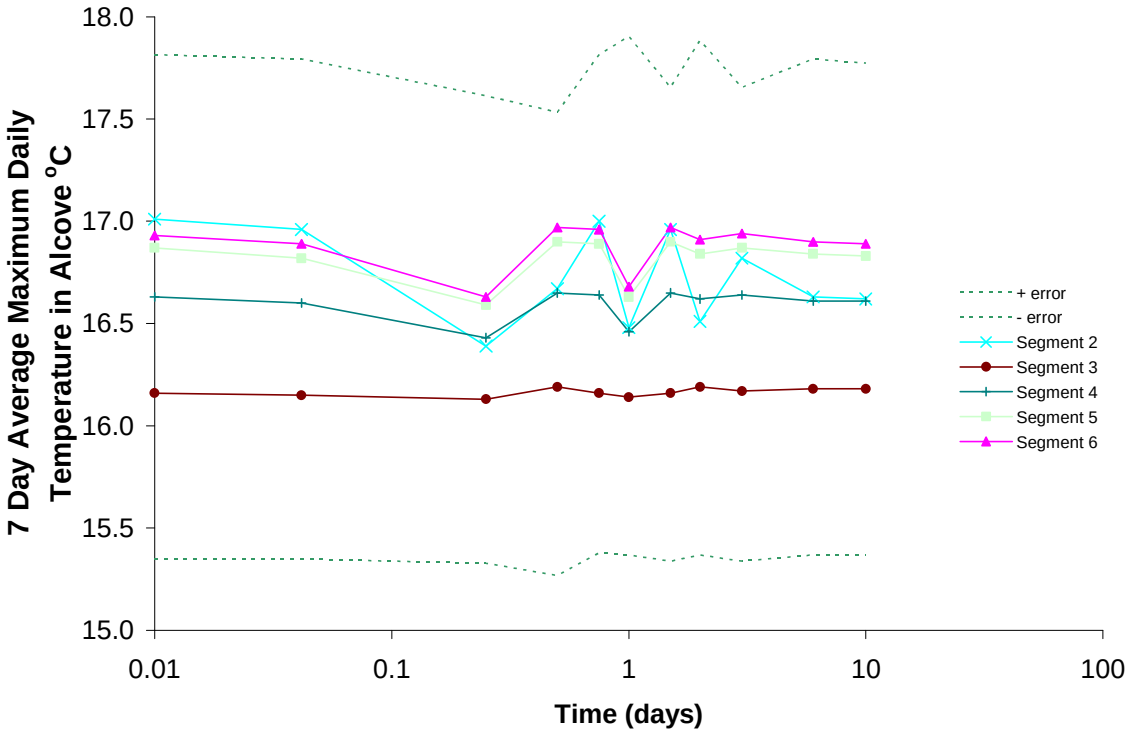

Figure 52. Green Island, effect of time lag on alcove temperature.

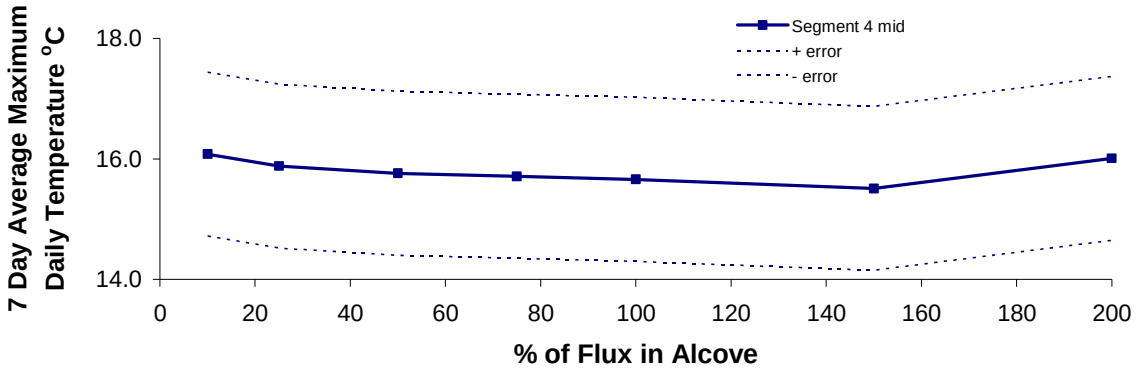

Figure 53. Norwood Slough, effect of flux on alcove temperature.

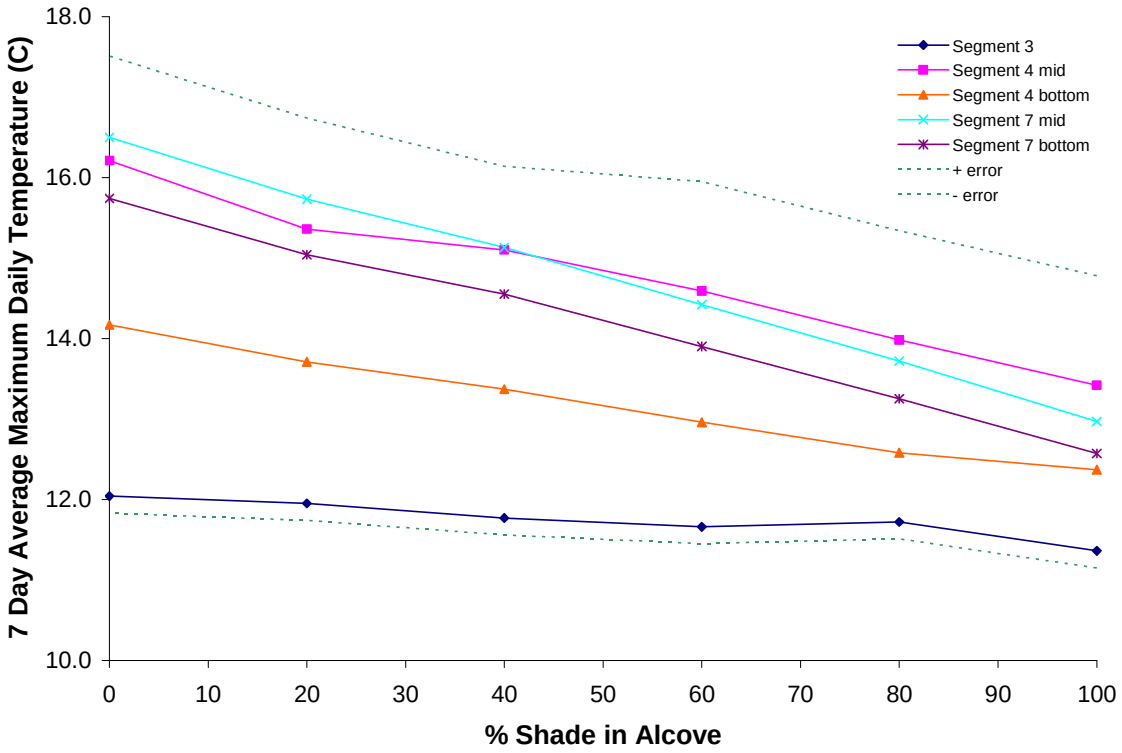

Figure 54. Norwood Slough, effect of shade on alcove temperature.

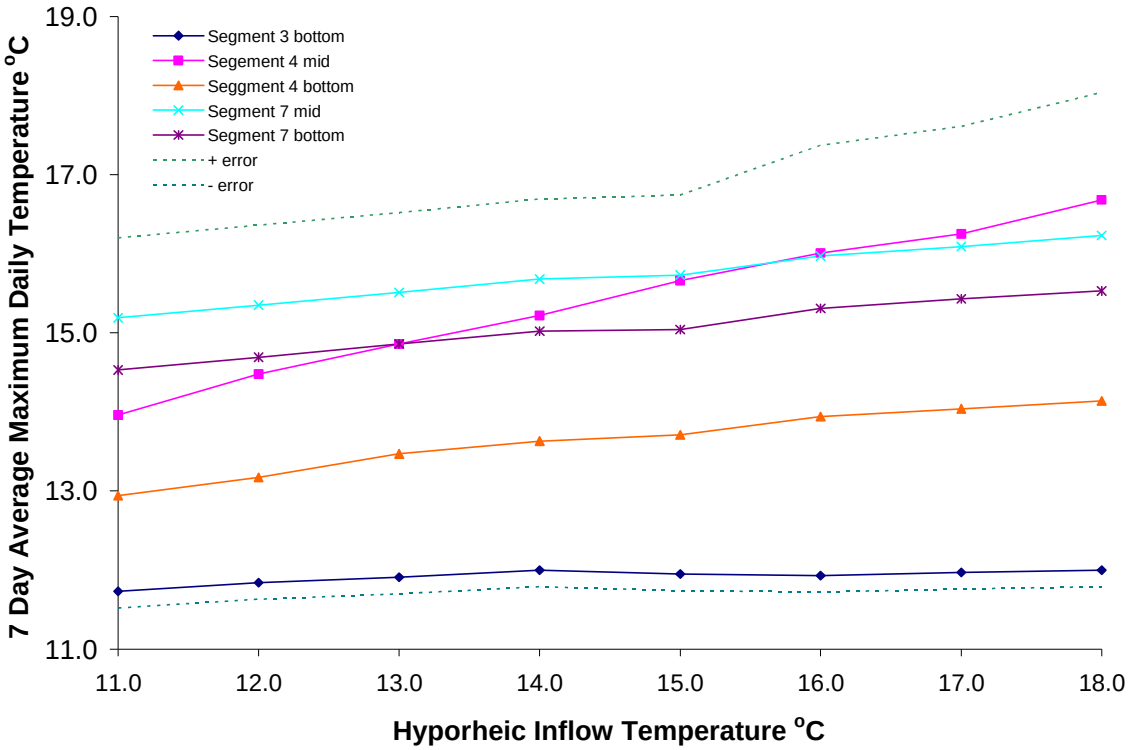

Figure 55. Norwood Slough, effect of hyporheic inflow temperature on alcove temperature.

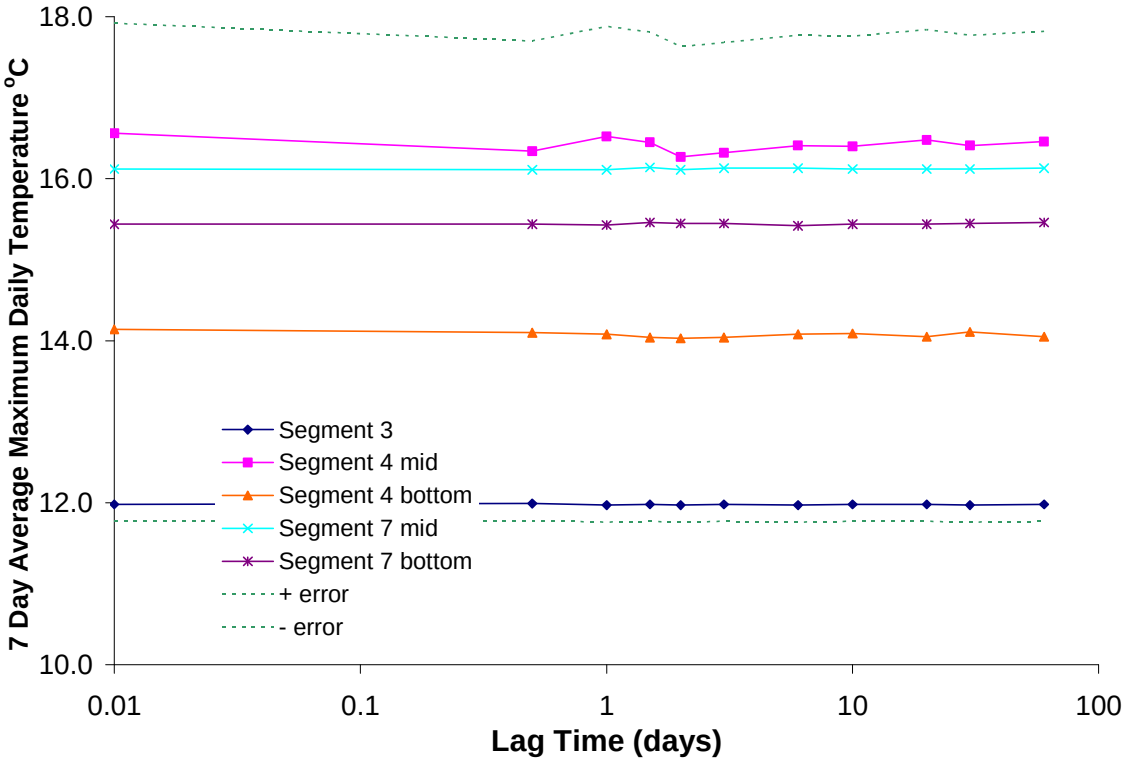

Figure 56. Norwood Slough, effect of lag time on alcove temperature.

9.2 Stallman Equation Graph

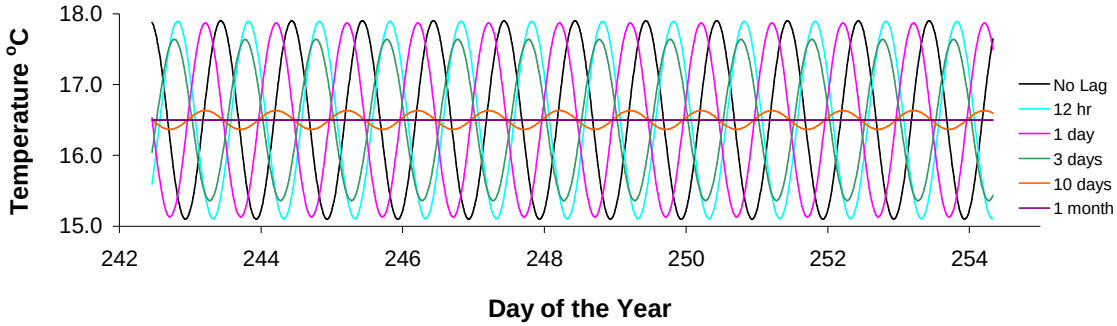

Figure 57. Harrisburg Bar, decay of mainstem temperature signal for different travel times.

10. APPENDIX E: FIELD, MODEL, AND SENSITIVY ANALYSIS DATA

Please see attached data CD for files.